UNIVERSITY OF KENT

SCHOOL OF NATURAL SCIENCES

Development of a Targeted Nucleic Acid Vector by Ring-Opening Metathesis Polymerisation of Norbornene-Ethidium Bromide Adducts and Supramolecular Self-Assembly of the Polymer into Fluorescent Nanoparticles

a thesis by

Patrick James Harte

BSc (Cantuar)

submitted in fulfilment of the
requirements for the degree of

Master of Science

by Research in Chemistry

AD MAIOREM DEI GLORIAM

In memory of Stephen Fell, a uniquely inspirational chemistry teacher with whom I had the privilege of performing laboratory experiments at Kent College, Canterbury for my A-Levels. In the short time that I knew him, Mr Fell uncovered within me a love of chemistry and a desire to study it further; it was this that kept me going through the disheartening setbacks that were numerous in my first year as a research student.

ACKNOWLEDGMENTS

I am grateful to my supervisors at the University of Kent, Drs Stefano Biagini and Chris Serpell, who led me through those setbacks with patience; they planned the direction of this project to begin with, and contributed substantially to the work by way of suggestion, explanation and correction. Dr Biagini has also been a great source of personal advice and comfort. Likewise, I thank those of my fellow researchers in the laboratory and elsewhere who offered theoretical and practical help, particularly Drs Dave Beal, Geraud Sansom and Sara Shehata.

Other individuals positively influenced my academic course, but were not involved in this work. Dr Maria Alfredsson—who guided me into the University of Kent and through my undergraduate years as my academic adviser—has long been a lifeline of emotional and administrative support. Jo Bradley, who taught me A-level chemistry, encouraged me to study the subject at university, helped me build my confidence as a student and was a friend to me when I had no other.

Finally, and most importantly, I am unrequitably indebted to my self-sacrificing parents, Jason and Adelina, who financed all of my studies and raised me in a privileged and nurturing environment. They and my siblings are the single constant throughout my life: the one group of people that I have always relied on the most, and who have never received the recognition that they deserve. I would not be here today without the love of my family.

ABSTRACT

Vectors are microscopic vehicles that can transport foreign nucleic acid sequences into a host cell, which is essential for genetic engineering processes such as molecular cloning and genome editing, with medical applications including gene therapy and vaccine development. Modifying the chemistry of the vector's exterior, so that it targets only specific cell types, is important for many applications. Most vectors are derived from biological sources, a well-known example being modified viruses, but this can cause adverse immune responses, so there is a need for entirely synthetic vectors.

Intercalation is the insertion of planar, aromatic small molecules between the base pairs of a DNA double helix. Many of these molecules fluoresce under ultraviolet light, enabling their use as nucleic acid stains in research, one of the most widely used being ethidium bromide (EthBr). This project aimed to develop an artificial vector consisting of polymeric nanoparticles, with specific exterior chemistry appropriate for cell targeting, and EthBr bonded to the interior: to intercalate DNA and trap it inside the nanoparticles, so that it can be transported and visualised.

Using cheap, commercially available materials, and standard, microwave and dry reaction conditions, the syntheses were conducted of a norbornene derivative and of various EthBr analogues—until one was found that was coupled successfully with the norbornene derivative. Compounds produced (some of them novel) were analysed extensively by melting point, infrared spectroscopy, gas and liquid chromatography–mass spectrometry and various nuclear magnetic resonance experiments.

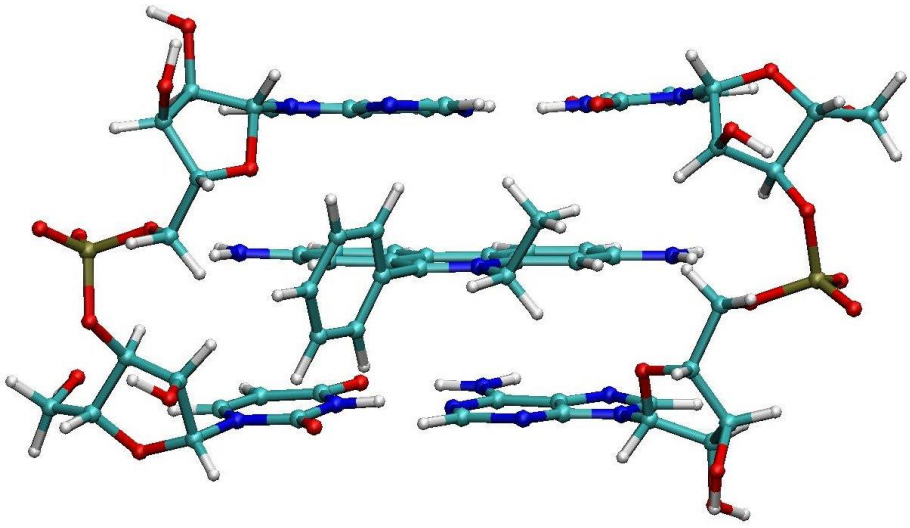

Figure 1: ethidium (centre) intercalated between two adenine-thymine DNA base pairs.[1]

TABLE OF CONTENTS

INTRODUCTION

AIM & OBJECTIVES

The aim of this project was to develop a novel kind of fluorescent vector that could encapsulate nucleic acids and direct their transport across cell membranes. To achieve this aim, seven instrumental objectives were advanced (see Figure 2). The first three were achieved in the project, the fourth one was accomplished by other members of the Biagini group, and the last three were not attempted due to lack of time.

1. Synthesis of a functionalisable monomer (i.e. a compound that later can be linked to the intercalator and then polymerised).
2. Synthesis of a functionalisable analogue of the chosen DNA intercalator (i.e. one that later can be linked to the monomer).
3. Covalent connection of the intercalator to the monomer via a linker.
4. Synthesis of a similar monomer, linked to PEG rather than the intercalator.
5. Co-polymerisation of these two monomers; self-assembly into nanoparticles.
6. Investigation of their fluorescence and intercalation of nucleic acids.
7. Investigation of their selectivity in transporting DNA across cell membranes.

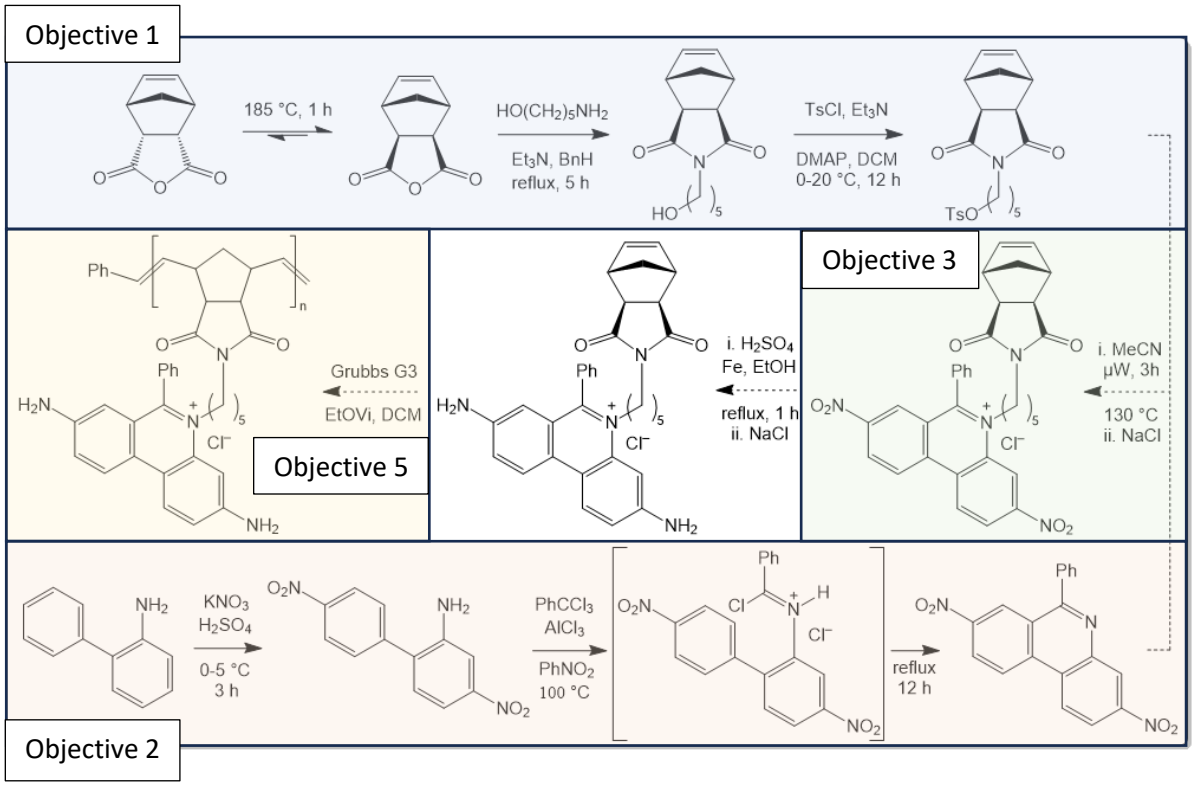

Figure 2: the original synthetic route to the intercalator monomer, followed by polymerisation.

This project relates to recent research by the Biagini group on the targeted delivery of chemotherapeutic drugs into cancer cells by encapsulating them in nanoparticles, which had hydrophobic exteriors and were self-assembled from block co-polymers of poly(ethylene glycol), abbreviated PEG, and drug-functionalised norbornenes.[2][3] This afforded control over the location of delivery, and timing of release (e.g. pH-triggered) of the therapeutic compound (see figure 3).

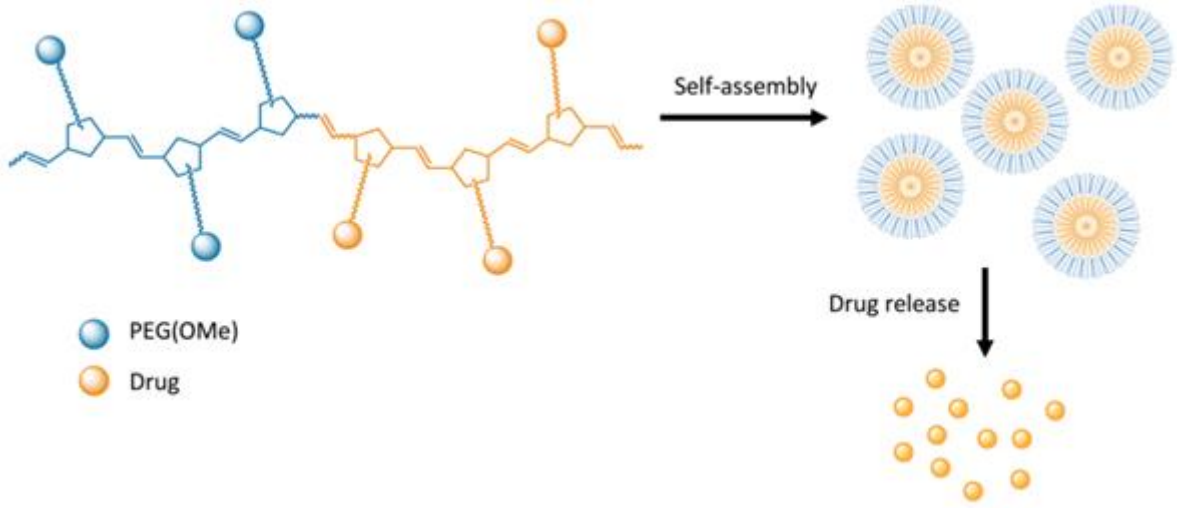

Figure 3: block co-polymer self-assembles into spherical aggregates; controlled drug release.[3]

This project was adapted from that work: its aim was to have a DNA intercalator molecule (instead of a drug) bonded to the interior of the nanoparticles. This would allow it to transport nucleic acids across cell membranes, which could have many important applications for cancer research and gene therapy.

Nucleic acid molecules are large, highly polar molecules that are unable—on their own—to pass through the non-polar lipid bilayer of a cell membrane, but they can be introduced into a cell by encapsulating them in a vehicle that is able to cross the membrane. There are several types of these vehicles (called 'vectors') that have been used, such as plasmids and viral vectors, but their applications are limited by safety concerns. Recently, some polymer-based vectors have been designed, with the nucleic acids loaded either by electrostatic attraction or by physically encapsulating them.[4]

The project described herein intended to encapsulate DNA inside nanoparticles self-assembled from block co-polymers consisting of units of PEG and of a moiety that can intercalate DNA, in this case derived from ethidium bromide (EthBr). PEG was chosen for co-polymers in earlier research by the Biagini group due to its solubility in water and its anticipated ability to facilitate passage across the cell membrane. The group has made block co-polymers using a type of living polymerisation technique called ROMP (see final section of introduction), which was used in this project too.

DNA INTERCALATORS

Deoxyribonucleic acid (DNA) is a natural biopolymer made up of two long, helically-coiled strands of phosphate-deoxyribose, bound together by hydrogen-bonding between complementary pairs of nucleobases: primarily cytosine with guanine and adenine with thymine (adenine with uracil in RNA). The sequential ordering of these base pairs encodes the genetic instructions for regulating the proper functioning and reproduction of all living cells.

Small molecules can interact with DNA either covalently or non-covalently; the former is irreversible and disables the DNA, causing cell death. The latter is usually reversible, and can be divided into four types, depending on which part of the DNA double helix they interact with: the phosphate backbone, the minor groove, the major groove, or between the base pairs.[5]

Those that insert themselves between the base pairs are intercalators (see figure 1). They are generally planar, polycyclic aromatics, which allows them to interact with the base pairs by π–π stacking, van der Waals and hydrophobic interactions, and makes many of them effective fluorophores.

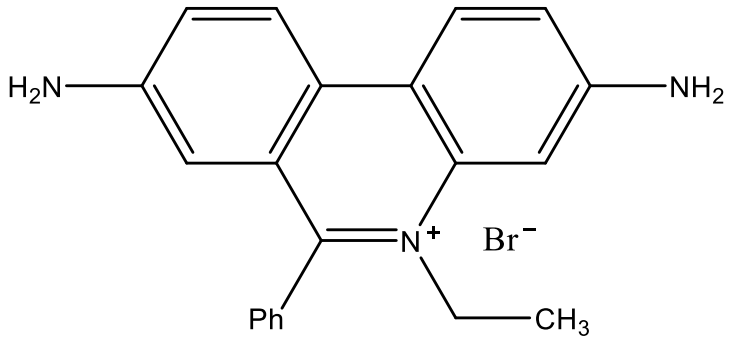

Figure 4: molecular structure of ethidium bromide (EthBr).

One of the most well-studied DNA intercalators is ethidium bromide (EthBr, see Figure 4), also known as homidium bromide.[6] It is commonly used by molecular biologists to stain and detect nucleic acids. For example, it is the predominantly-used tag for staining DNA in agarose gel electrophoresis, whereby a mixture of DNA fragments is separated by length.[7]

On irradiation with ultraviolet light, EthBr fluoresces orange, but it does so twenty times brighter when intercalating DNA. Unlike other common intercalators, such as proflavine and doxorubicin, which are mutagenic and toxic due to their DNA-disrupting effects, EthBr is relatively safe, despite its undeserved reputation as a mutagen.

TYPES OF POLYMERIZATION

There are two main classes of polymerisation: chain-growth and step-growth (see figure 5). Living polymerisation is a form of chain-growth.

Chain-growth polymerisation proceeds by the continuous addition of monomer units onto the ends of polymer chains, which grow at a linear rate. First, an initiator molecule decomposes to form an activated species (initiation). Then this species reacts with the monomer, forming the beginnings of a polymer chain, with an active site; in the same way, more monomers add on to the chain at this active site (propagation). Finally, the active site is deactivated, and the chain stops growing (termination).

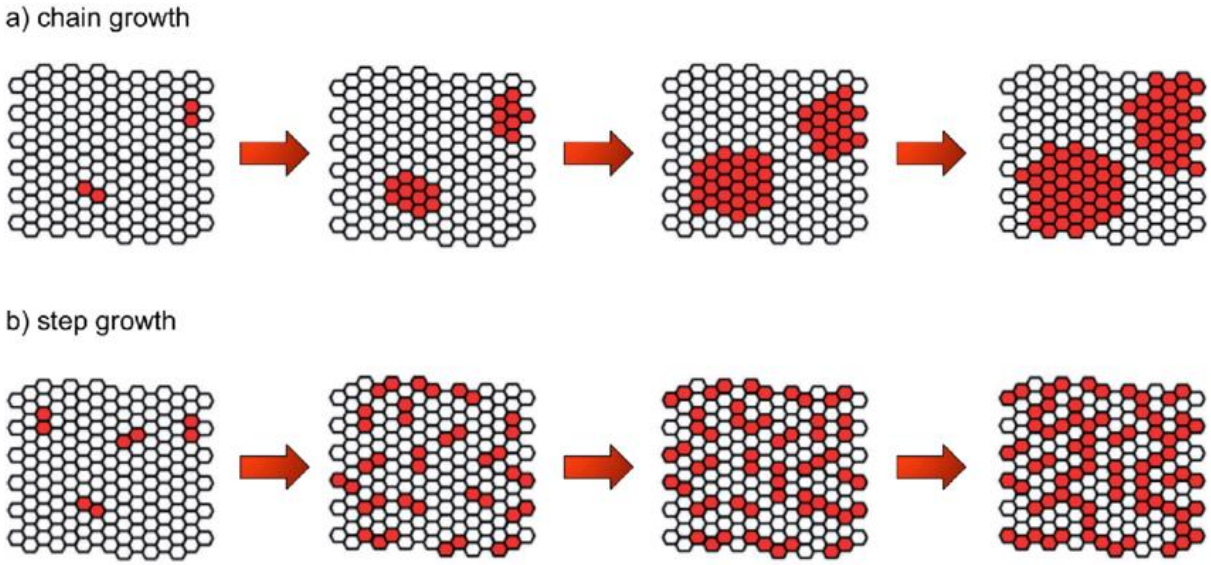

Figure 5: comparison of chain growth and step growth.[8]

In step-growth polymerisation, bi-functional (or multifunctional) monomers react together to form dimers, which in turn react with more monomer or with each other to form longer oligomers, and then longer and longer polymers. Almost all of the monomer is exhausted very early in the process, but long chain lengths only begin to be formed at nearly 100% monomer conversion (which is very difficult to achieve).

Living polymerisation is a type of chain-growth in which the termination step cannot happen spontaneously. Propagation continues until all the monomer is exhausted, but even then, the reaction is still "alive" and will resume if more monomer is added.[9] This makes it very convenient for synthesising block co-polymers, by adding the desired amounts of each monomer separately in stages. The reaction is only terminated when the initiator is quenched. Living polymerisation affords fine control over the average molecular weight of the resulting polymer, low dispersity in molecular weight (deviation from the mean, i.e. little variation in weight), and control over the end groups of the polymer.

BLOCK CO-POLYMERS

In order to self-assemble into nanoparticles, the polymer molecules need to have an appropriate chemical structure. This is similar to the way that soap works: it uses a kind of compound called an emulsifier that consists of a hydrophilic head group (generally a carboxylate salt) bonded to a hydrophobic tail group (usually a fairly long alkyl chain). Favourable intermolecular interactions cause the head groups of adjacent molecules to self-associate, and the tail groups to do likewise. If the soap is mixed with a large quantity of water, the hydrophobic heads will interact with the water (as well as with each other) while the tail groups will only interact with each other. In order to maximise the opportunities for these favourable interactions (head-head, head-water and tail-tail), and to minimise unfavourable ones (head-tail and tail-water), the molecules can self-assemble into loosely-bound spherical aggregates called micelles. These nanoscopic particles will arrange themselves (in aqueous media) so that the head groups all face outwards—towards the water—and all the tail groups face inwards, away from the water. Lipophilic substances (e.g. fat, oil or grease) that normally would not mix with water and are thus difficult to wash away with water alone, diffuse into the centre of these micelles (with the help of some agitation, e.g. the rubbing together of hands) and become trapped there. The micelles—and their greasy contents—are thus carried away by running water, due to attractive electrostatic forces between the water and the head groups.

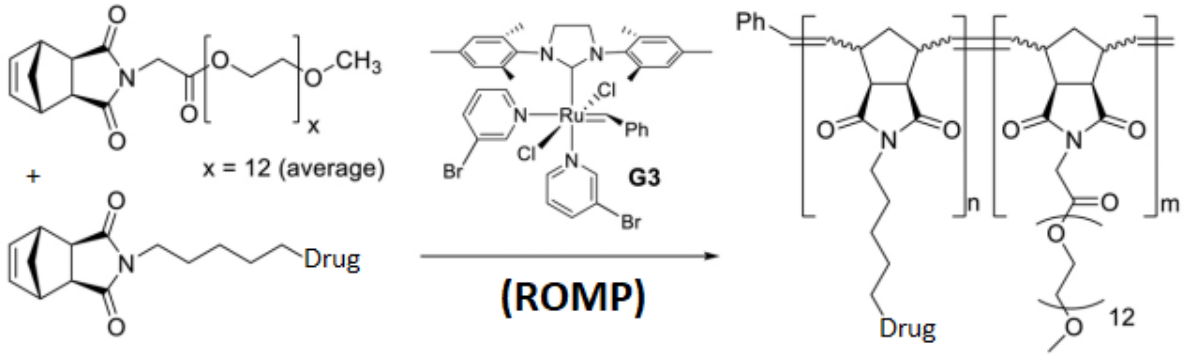

Figure 6: co-polymerisation of norbornene-based monomers, one linked to PEG, the other to a drug.

Likewise, the polymer needed an appropriate structure to enable self-assembly into nanoparticles. The Biagini group previously formed a block co-polymer in an "AB" arrangement, so that each polymer chain consisted of two discrete sections: all of the polyethylene glycol (PEG)-substituted units constituted the hydrophilic end and all of the drug-substituted units were at the other end (see figure 6).[3] PEG was chosen for this project too because it enables self-assembly, as described above. The other end needed to be hydrophobic, which influenced the choice of fluorescent DNA intercalator: EthBr is well-studied and relatively non-polar.

RING-OPENING METATHESIS POLYMERISATION (ROMP)

Ring-opening polymerisation (ROP) propagates by the attack of an active chain end on a cyclic monomer, thus it is a form of chain-growth polymerisation. Like other kinds of polymerisation, ROP is entropically disfavoured, because it involves many small molecules coming together to make a few very large ones, thus decreasing the degrees of freedom of the system. However, this negative entropy change is relatively small compared to the large enthalpic change that drives the reaction: the release of bond-angle strain from opening the ring. Ergo the monomer must be cyclic and its ring needs sufficiently small bond angles to make it quite strained, which is usually achieved by having five members or fewer.

Ring-opening metathesis polymerisation (ROMP) is a kind of ROP that uses a cycloalkene as the monomer. Its propagation mechanism is an olefin metathesis: two alkenes come together to form a four-membered ring intermediate, which then breaks to form two new alkenes, with the carbon atom pairings swapped (see figure 7). Most kinds of olefin metathesis are (at least partly) entropically-driven by the evolution of a gaseous small molecule by-product such as ethylene or propylene. ROMP is different: the monomer is a cyclic alkene, so the two new alkenes formed are separate parts of the same molecule (the polymer chain), thus there is no such by-product, and the driving force is enthalpic, as mentioned above.

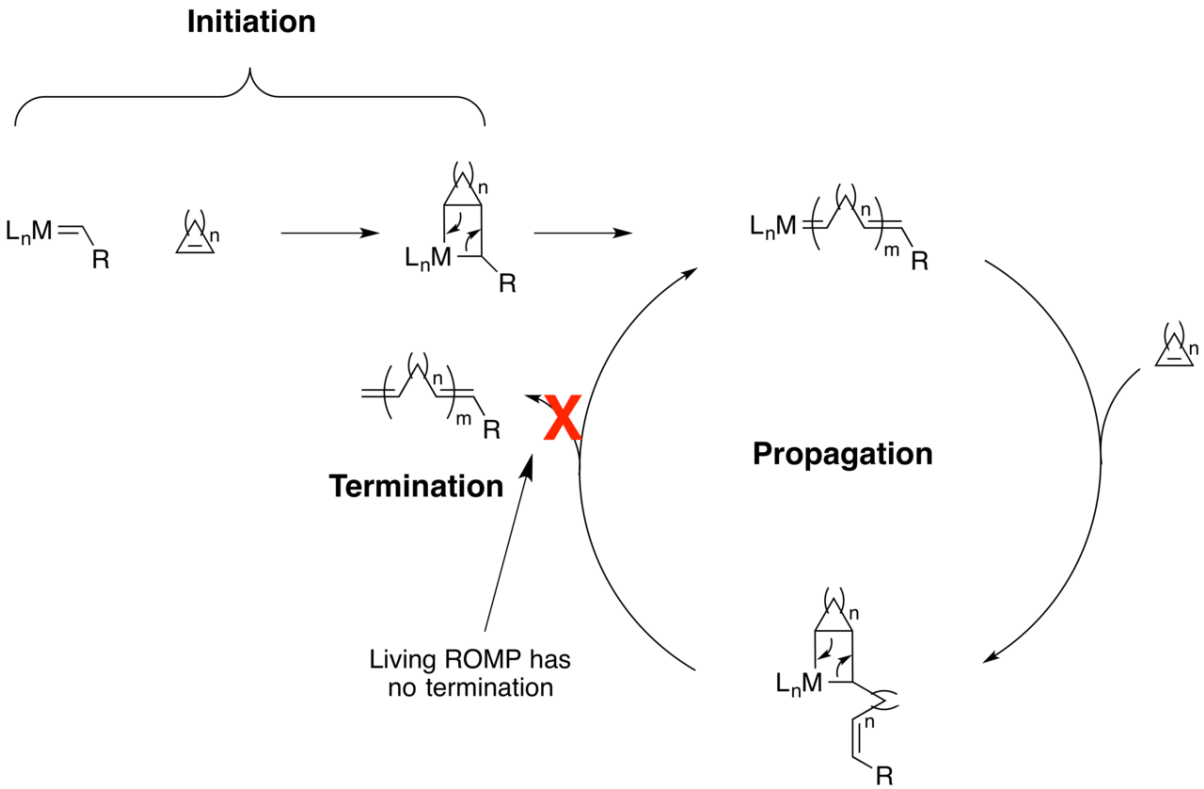

Figure 7: general reaction steps in ROMP.[10]

Under the right conditions, ROMP can be a living polymerisation, with all the aforementioned advantages thereof.[11] For this to be the case, the catalyst needs to be active enough to provide a fast rate of initiation, relative to the rate of propagation. Therefore, the degree of polymerisation (average number of monomer units in a polymer chain) is directly proportional to the initial quantity of monomer, and because all the chains start growing at roughly the same time, they are all of very similar lengths (dispersity <1.5). The third generation Grubbs catalyst (G3) has a much faster rate of initiation than its predecessors and a dispersity index <1.1, while also being tolerant of a variety of monomer chemistries.[12] However, it must be stored under nitrogen and used before it oxidises.

As previously explained, ROMP works on any sufficiently strained cycloalkene monomer, including cyclopentene. However, to make it a living polymerization requires a fast initiation rate, so it helps to choose a monomer that is very reactive. Bicyclic and tricyclic alkenes (particularly those with bridged ring systems) can have very strained bond angles, which makes them easier to polymerise than monocyclic ones, and affords a broader choice of catalysts. They also leave behind a ring in the repeat unit of the polymer chain, thereby making the polymer backbone relatively rigid, and hindering it from curling up on itself.

Norbornene, which is systematically named bicyclo[2.2.1]hept-2-ene, forms the hydrocarbon core of some of the most commonly used monomers for ROMP. This hydrocarbon itself is of little use outside the rubber industry, but various derivatives have been studied, usually functionalised at positions two and/or three. One such derivative, with which our research group has enjoyed success, and which was used in this project, is himic anhydride. Also known as carbic (or nadic) anhydride or semi-systematically as *cis*-5-norbornene-2,3-dicarboxylic anhydride, it is readily produced by a Diels-Alder reaction between cyclopentadiene and maleic anhydride, and is commercially available at low cost. However, two isomers exist—*endo* and *exo*—that exhibit some differences in their chemical properties. The *endo* diastereomer is cheaper, being the major product of the aforementioned reaction, but it does not polymerise well due to steric clashes. It is therefore necessary to obtain *exo*-himic anhydride by thermal isomerisation, which has a yield of no more than 60%, followed by serial recrystallisation.[13]

The Biagini group has also investigated the potential of fluorescent ROMP polymers previously, with a monomer containing Rhodamine B having been successfully co-polymerized and self-assembled.[14]

EXPERIMENTAL

Assignments are given using the arbitrarily-numbered molecular structures adjacent to the data; this numbering scheme does not necessarily correspond to the IUPAC system. NMR splitting patterns are signified in this work using the following abbreviations: s (singlet), d (doublet), t (triplet), q (quartet), p (pentet), x (sextet), h (heptet), o (octet), n (nonet), m (multiplet), a (apparent, indicating loss of complexity due to almost-identical coupling constants), b (broad) and c (complex, indicating visible but unresolved higher-order splitting). To exemplify the distinction between 'apparent' and 'complex': if a proton couples to two protons that are in different environments but with very similar *J*, then the signal may be described as an apparent triplet instead of a doublet of doublets; whereas if the values of *J* are different but one of them is too small to be measured, then the signal may be called a complex doublet.

ISOMERISATION OF HIMIC ANHYDRIDE {***n*1→*x*1}**

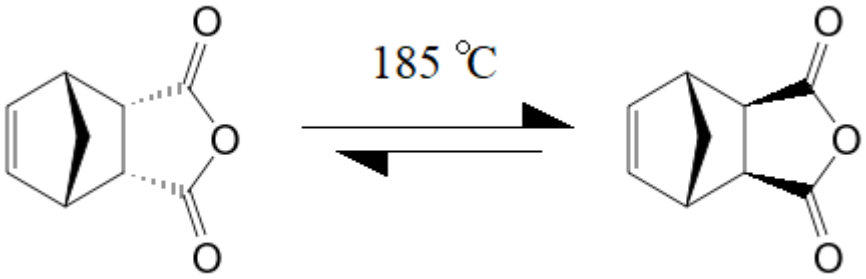

Figure 8: thermal isomerisation of *endo*-himic anhydride {***n*1**} to *exo*-himic anhydride {***x*1**}.

Endo-himic anhydride {***n*1**} (51.55 g, 314 mmol) was heated to 185(±10) °C for three hours (see figure 8). A heat gun was used to melt some of the material that had sublimed and re-deposited on the upper hemisphere of the flask. The crude product was left to cool for a few minutes (with the heating mantle set to 111 °C) until it started to freeze, at which point it was dissolved in the minimum volume of toluene under reflux. A small amount of insoluble dark solid was removed by hot filtration after the addition of extra toluene, then the filtrate was concentrated *in vacuo* and redissolved in the minimum volume under reflux. The solution was left overnight to cool at room temperature. After 16-20 hours white crystals had formed, although the crystals at the very bottom of the flask formed a single, compact, beige-coloured mass, which was manually separated and discarded. The recrystallisation was repeated twice more—without hot filtration—yielding *cis*-5-norbornene-*exo*-2,3-dicarboxylic anhydride {***x*1**} (5.60 g, 34.1 mmol, 10.9% yield) of 97.9% purity, as determined by GC-MS.

Analysis of *exo*-himic anhydride {***x*1**}

M.P. 140–142 °C. Lit: 141–144 °C,[15] 140–142 °C.[16][17]

^{1}H NMR (400 MHz, $CDCl_3$) δ/ppm: 6.34 (**1'**, 2H, at, *J*=1.7 Hz); 3.47 (**2'**, 2H, ap, *J*=1.7 Hz); 3.01 (**4'**, 2H, d, *J*=1.6 Hz); 1.68 (**3'**, 1H, dt, *J*=10.2, 1.6 Hz); 1.46 (**3"**, 1H, dap, *J*=10.2 Hz). See figure 9 and figure 10.

^{13}C NMR (400 MHz, $CDCl_3$) δ/ppm: 171.6 (**3**); 137.9 (**4**); 48.7 (**1**); 46.8 (**2**); 44.1 (**5**). See figure 9 and figure 11.

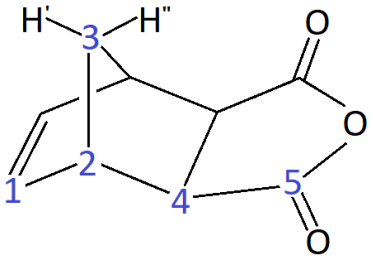

Figure 9: arbitrarily numbered structure of *exo*-himic anhydride {***x*1**}.

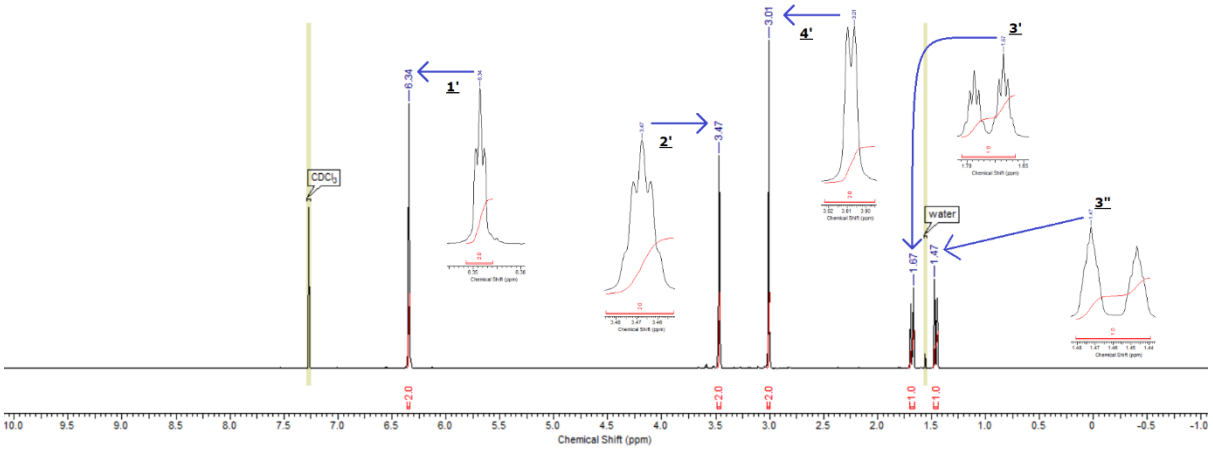

Figure 10: ^{1}H NMR of *exo*-himic anhydride {***x*1**}.

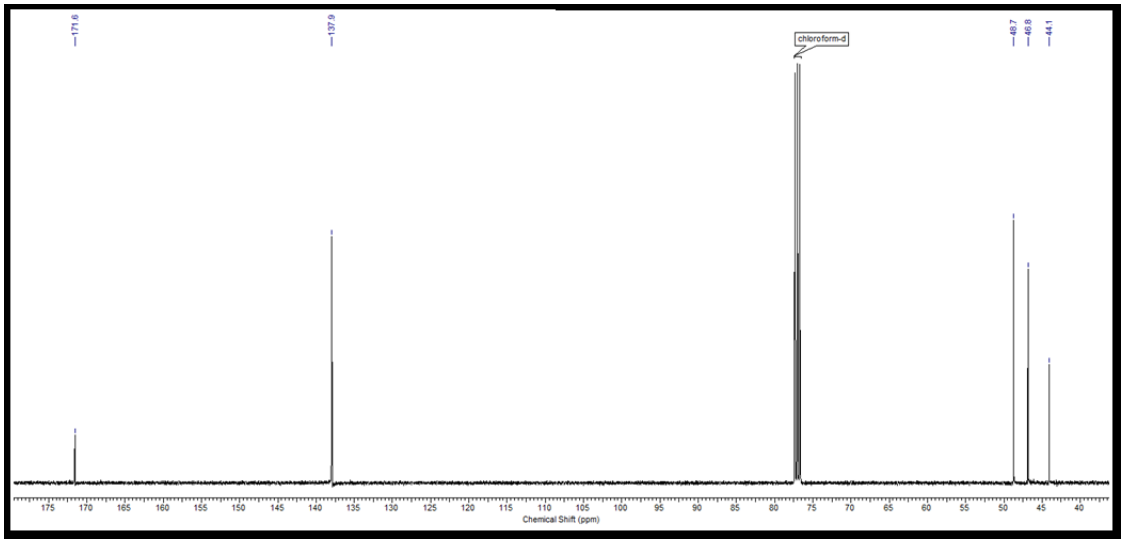

Figure 11: ^{13}C NMR of *exo*-himic anhydride {***x*1**}.

IMIDIZATION OF HIMIC ANHYDRIDE {1→2}

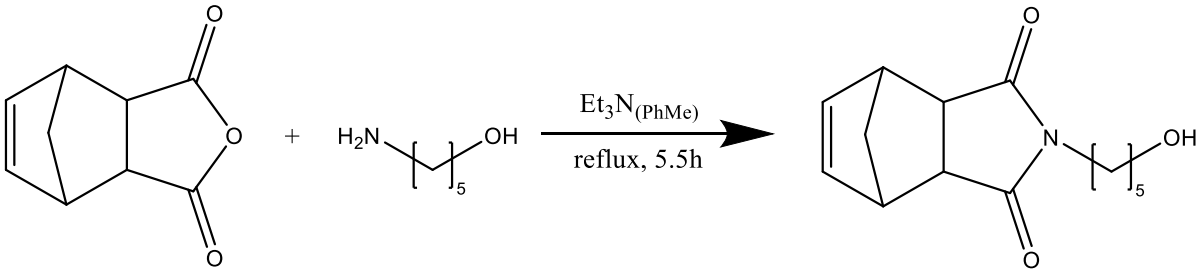

Figure 12: himic anhydride {**1**} reacts with 5-aminopentanol {**AP**} to form a himidol {**2**}.

The same procedure was used to produce both diastereomers of the himidol {**2**}, in separate reactions but with the same quantities used each time, the only difference being the isomerism of the starting material and product. As expected, *endo*-himic anhydride {***n*1**} yielded *endo*-himidol {***n*2**}, and *exo*-himic anhydride {***x*1**} yielded *exo*-himidol {***x*2**}. Himic anhydride {**1**} (1.00 g, 6.09 mmol) and triethylamine (85 µL) were dissolved in toluene (25 mL) with gentle heating, then 5-aminopentanol {**AP**} (660 mg, 6.40 mmol) was added and the solution was heated under reflux for five and a half hours (see figure 12). The reaction was monitored by TLC in ethyl acetate—stained with ethanolic phosphomolybdic acid (0.1 g/mL), then heated with a heat gun. The crude product was concentrated *in vacuo*, dissolved in DCM (20 mL), washed twice with HCl (2×10 mL, 1 M), twice with water (2×10 mL), dried over $MgSO_4$ and again concentrated *in vacuo* to a yellow oil, then purified by flash chromatography in ethyl acetate, yielding a pale yellow oil. Most of the crude *endo* product was never purified because it was not needed, so the yield of N-(5-hydroxypentyl)-*cis*-5-norbornene-*endo*-2,3-dicarboximide {***n*2**} (329 mg, 22%) is lower than it otherwise would be. All of the *exo* product {***x*2**}, N-(5-hydroxypentyl)-*cis*-5-norbornene-*exo*-2,3-dicarboximide (735 mg, 48%) was purified.

Analysis of N-(5-hydroxypentyl)-*endo*-himide {*n*2}

M.P. not measured (liquid under ambient conditions).

IR ν_{max}/cm^{-1}: 3447 (hydroxyl O–H ν, b); 2940 (alkyl C–H ν, w); 2866 (alkyl C–H ν, w); 1763 (cyclic imide C=O ν, w); 1682 (cyclic imide C=O ν, s). See figure 16.

^{1}H NMR (400 MHz, $CDCl_3$) δ/ppm: 6.08 (**1'**, 2H, at, *J*=1.9 Hz); 3.60 (**10'**, 2H, t, *J*=6.5 Hz); 3.37 (**2'**, 2H, ao, *J*=1.7 Hz); 3.32 (**6'**, 2H, t, *J*=7.6 Hz); 3.23 (**4'**, 2H, dd, *J*=2.9, 1.6 Hz); 1.82 (**10"**, 1H, bs); 1.72 (**3'**, 1H, dt, *J*=8.8, 1.6 Hz); 1.53 (**9'**, **3"**, 3H, m); 1.45 (**7'**, 2H, ap, *J*=7.6 Hz); 1.30 (**8'**, 2H, m). See figure 13 and figure 14.

^{13}C NMR (400 MHz, $CDCl_3$) δ/ppm: 177.9 (**5**); 134.4 (**1**); 62.6 (**10**); 52.3 (**3**), 45.7 (**4**), 44.9 (**2**), 38.2 (**6**), 32.1 (**9**), 27.5 (**7**), 23.0 (**8**). See figure 13 and figure 15.

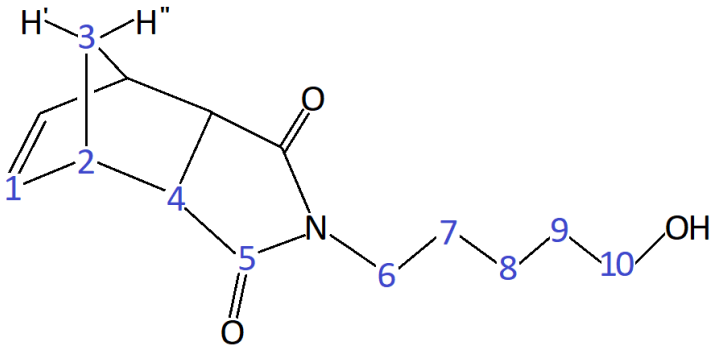

Figure 13: arbitrarily numbered structure of N-(5-hydroxypentyl)-*endo*-himide {***n2***}.

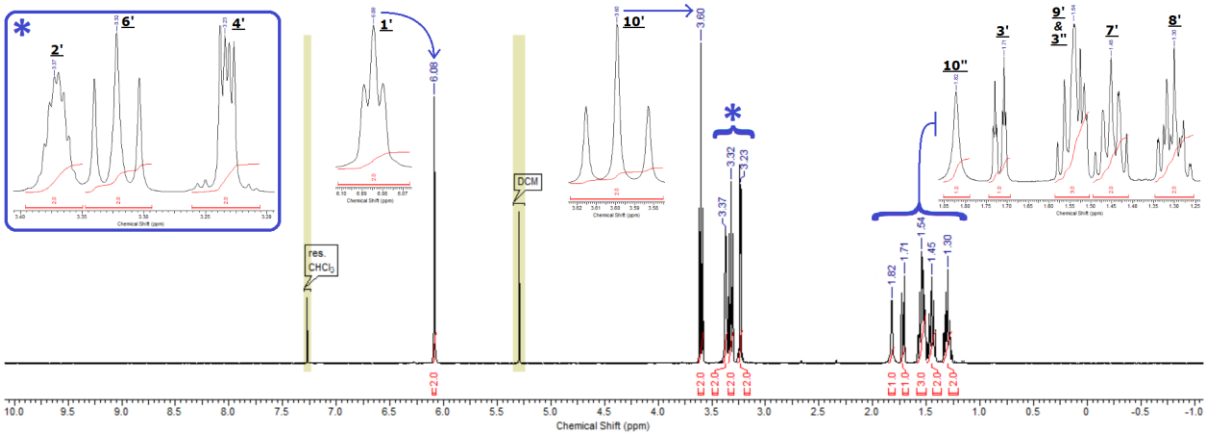

Figure 14: ^{1}H NMR of N-(5-hydroxypentyl)-*endo*-himide {***n2***}.

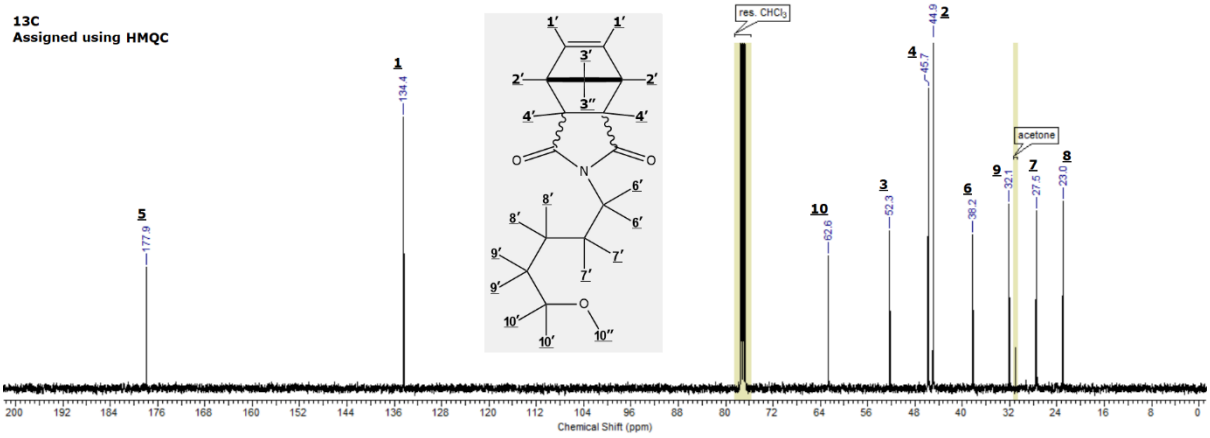

Figure 15: ^{13}C NMR of N-(5-hydroxypentyl)-*endo*-himide {***n2***}.

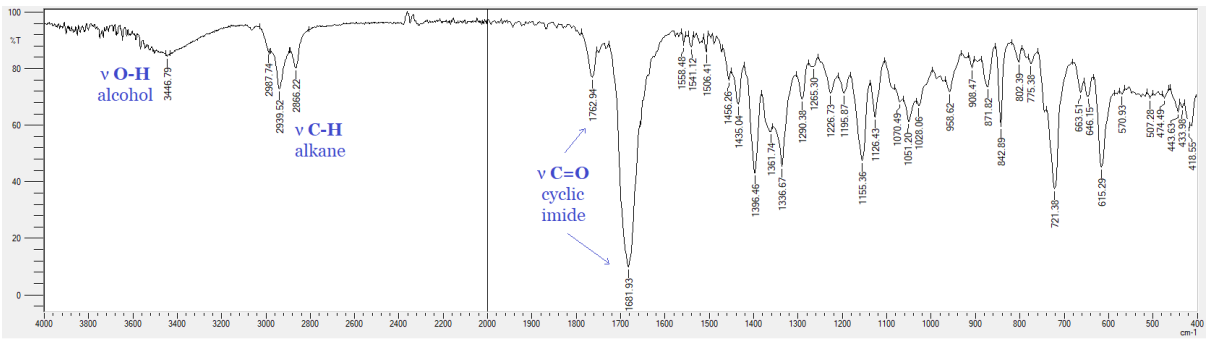

Figure 16: FT-IR of N-(5-hydroxypentyl)-*endo*-himide {***n2***}.

Analysis of N-(5-hydroxypentyl)-*exo*-himide {*x*2}

M.P. not measured (liquid under ambient conditions).

IR ν_{max}/cm^{-1}: 3447 (hydroxyl O–H ν, b); 2940 (alkyl C–H ν, w); 2864 (alkyl C–H ν, w); 1767 (cyclic imide C=O ν, w); 1684 (cyclic imide C=O ν, s). See figure 19.

^{1}H NMR (400 MHz, $CDCl_3$) δ/ppm: 6.28 (**1'**, 2H, at, *J*=1.8 Hz); 3.63 (**10'**, 2H, t, *J*=6.4 Hz); 3.47 (**6'**, 2H, t, *J*=7.4 Hz); 3.27 (**2'**, 2H, ap, *J*=1.6 Hz); 2.67 (**4'**, 2H, d, *J*=1.4 Hz); 1.98 (**10"**, 1H, bs); 1.59 (**9'**, **7'**, 4H, m); 1.51 (**3'**, 1H, dt, *J*=9.8, 1.5 Hz); 1.37 (**8'**, 2H, m); 1.22 (**3"**, 1H, cd, *J*=9.8 Hz). See figure 17 and figure 18.

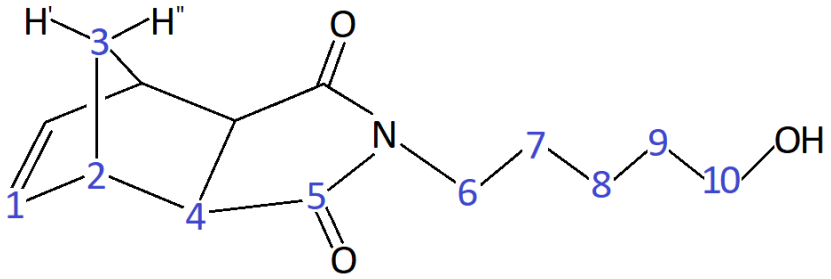

Figure 17: arbitrarily numbered structure of N-(5-hydroxypentyl)-*exo*-himide {***x*2**}.

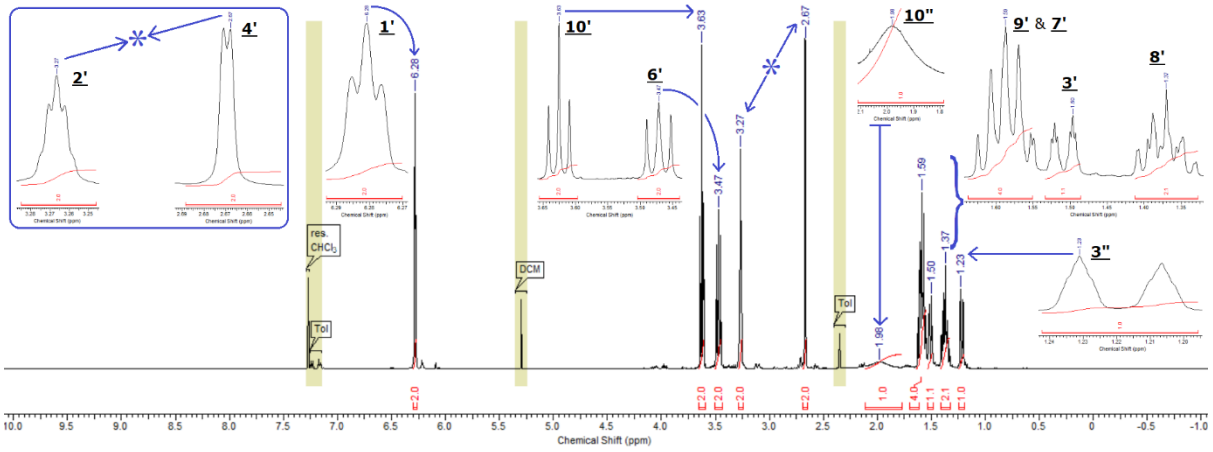

Figure 18: ^{1}H NMR of N-(5-hydroxypentyl)-*exo*-himide {***x*2**}.

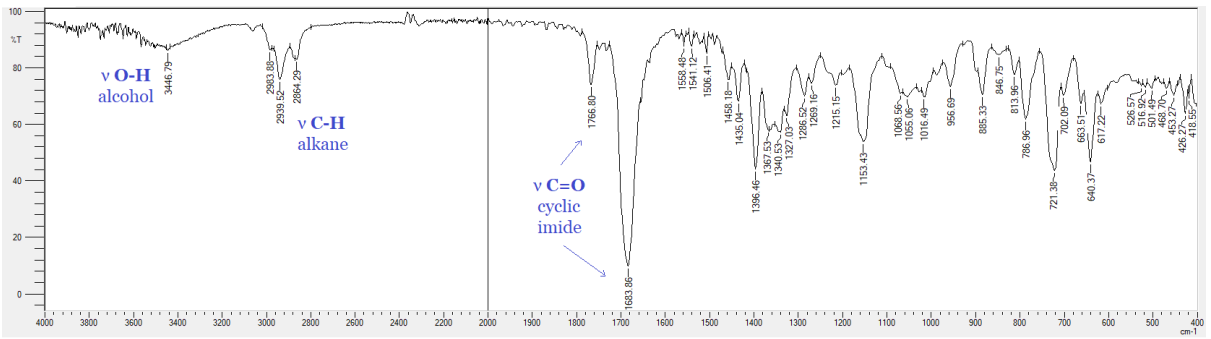

Figure 19: FT-IR of N-(5-hydroxypentyl)-*exo*-himide {***x*2**}.

TOSYLATION OF HIMIDOL {2→3}

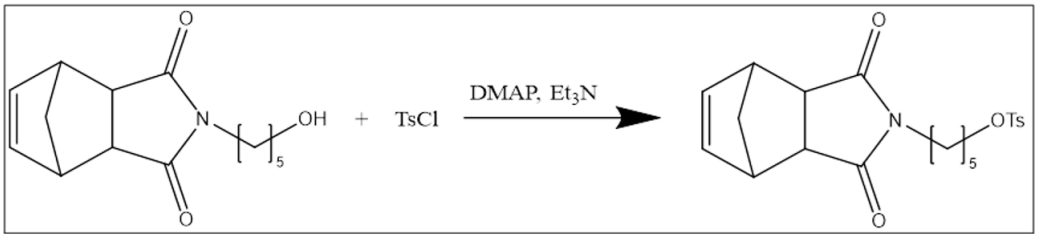

Figure 20: tosylation of himidol {**2**} to himide-tosylate {**3**}.

Like the imidization, the tosylation was duplicated using equal quantities. N-(5-hydroxypentyl)-himide (500 mg, 2.01 mmol) and DMAP (24.5 mg, 0.20 mmol) were dissolved in dry DCM (100 mL). Triethylamine (560 µL, 4.01 mmol) was added under an atmosphere of nitrogen. The mixture was cooled to −10 °C, then tosyl chloride was added slowly with gentle stirring, keeping the temperature around 0 °C. The reaction was monitored by TLC and left overnight at room temperature. It was washed with 10 % citric acid solution, then saturated sodium bicarbonate solution, then water (2×20 mL each). The product was dried over magnesium sulfate and concentrated *in vacuo*, yielding N-(5-tosylatopentyl)-*cis*-5-norbornene-*endo*-2,3-dicarboximide {***n*3**} (590 mg, 73%) and the *exo* diastereomer {***x*3**} (see figure 20).

Analysis of N-(5-tosylatopentyl)-*endo*-himide {*n*3}

M.P. 54–57 °C.

IR ν_{max}/cm^{-1}: 2943 (alkyl C–H ν, w); 2868 (alkyl C–H ν, w); 1767 (cyclic imide C=O ν, w); 1690 (cyclic imide C=O ν, s); 1597 (arene C≈C β, w); 1354 (sulfonate S=O ν, m); 1173 (C–O ν, s); 721 (*cis*-vinylene C=C β, m). See figure 23.

^{1}H NMR (400 MHz, $CDCl_3$) δ/ppm: 7.78 (**12'**, 2H, dat, *J*=8.3, 1.8 Hz); 7.35 (**13'**, 2H, cd, *J*=8.2 Hz); 6.07 (**1'**, 2H, at, *J*=1.8 Hz); 3.99 (**10'**, 2H, t, *J*=6.3 Hz); 3.38 (**2'**, 2H, ao, *J*=1.7 Hz); 3.28 (**6'**, 2H, t, *J*=7.2 Hz); 3.23 (**4'**, 2H, dd, *J*=2.9, 1.5 Hz); 2.46 (**15'**, 3H, s); 1.73 (**3'**, 1H, dt, *J*=8.8, 1.6 Hz); 1.63 (**9'**, 2H, ap, *J*≈7 Hz); 1.54 (**3"**, 1H, cd, *J*=8.7 Hz); 1.40 (**7'**, 2H, ap, *J*≈7.5 Hz); 1.27 (**8'**, 2H, m). Figure 21 and figure 22.

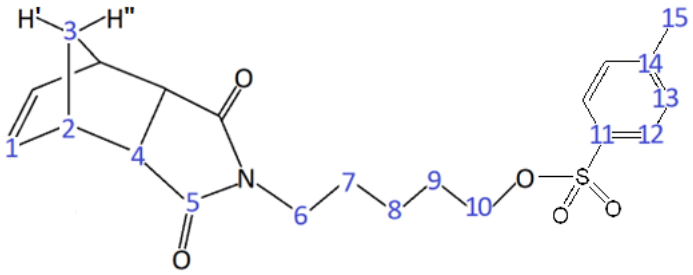

Figure 21: arbitrarily numbered structure of N-(5-tosylatopentyl)-*endo*-himide {***n*3**}.

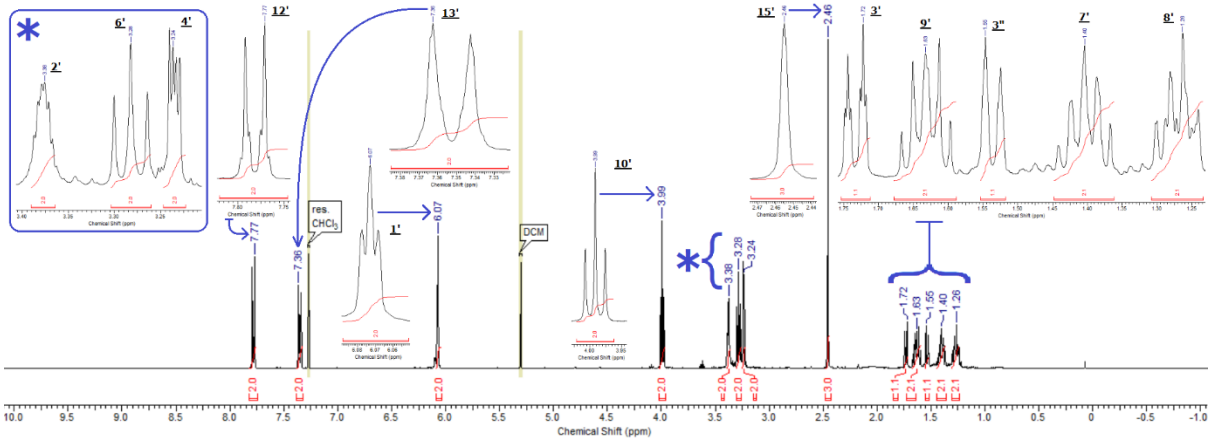

Figure 22: ^{1}H NMR of N-(5-tosylatopentyl)-*endo*-himide {***n*3**}.

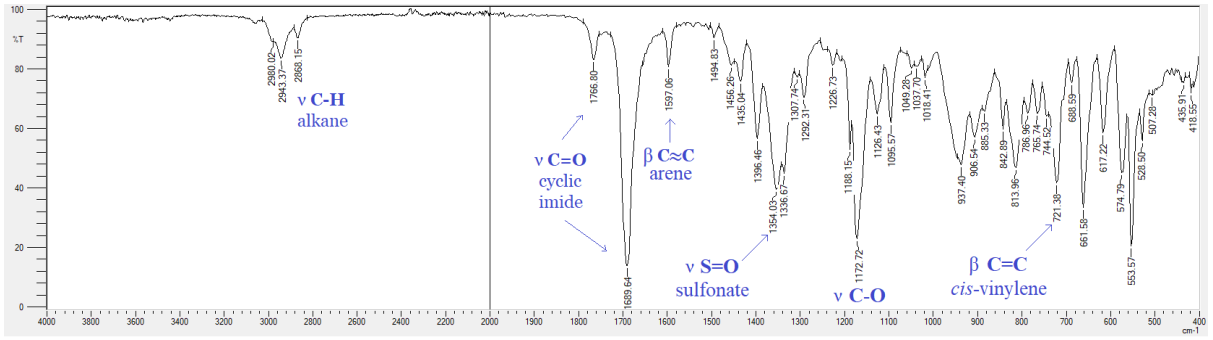

Figure 23: FT-IR of N-(5-tosylatopentyl)-*endo*-himide {***n*3**}.

Analysis of N-(5-tosylatopentyl)-*exo*-himide {*x*3}

^{1}H NMR (400 MHz, $CDCl_3$) δ/ppm: 7.77 (**12'**, 2H, dat, *J*=8.3, 1.8 Hz); 7.35 (**13'**, 2H, cd, *J*=8.2 Hz); 6.28 (**1'**, 2H, at, *J*=1.7 Hz); 4.00 (**10'**, 2H, t, *J*=6.4 Hz); 3.41 (**6'**, 2H, t, *J*=7.3 Hz); 3.25 (**2'**, 2H, at, *J*=1.6 Hz); 2.66 (**4'**, 2H, d, *J*=1.1 Hz); 2.45 (**15'**, 3H, s); 1.66 (**9'**, 2H, ap, *J*≈7 Hz); 1.51 (**7'**, **3'**, 3H, m); 1.31 (**8'**, 2H, m); 1.18 (**3"**, 1H, cd, *J*=9.9 Hz). See figure 24 and figure 25.

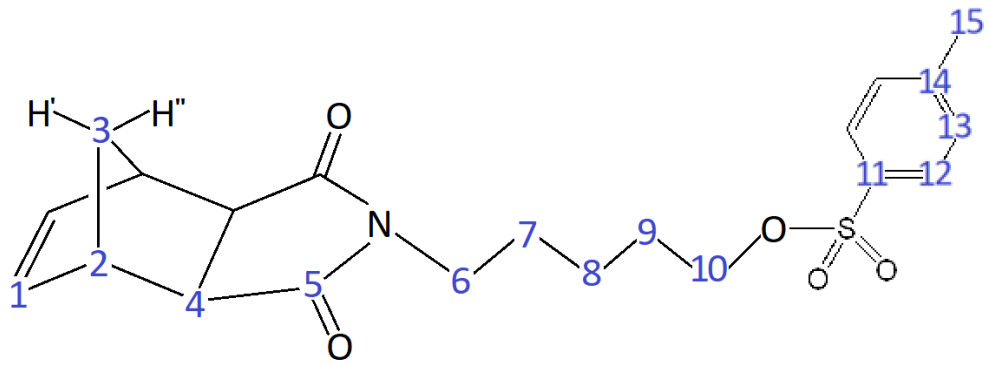

Figure 24: arbitrarily numbered structure of N-(5-tosylatopentyl)-*exo*-himide {***x*3**}.

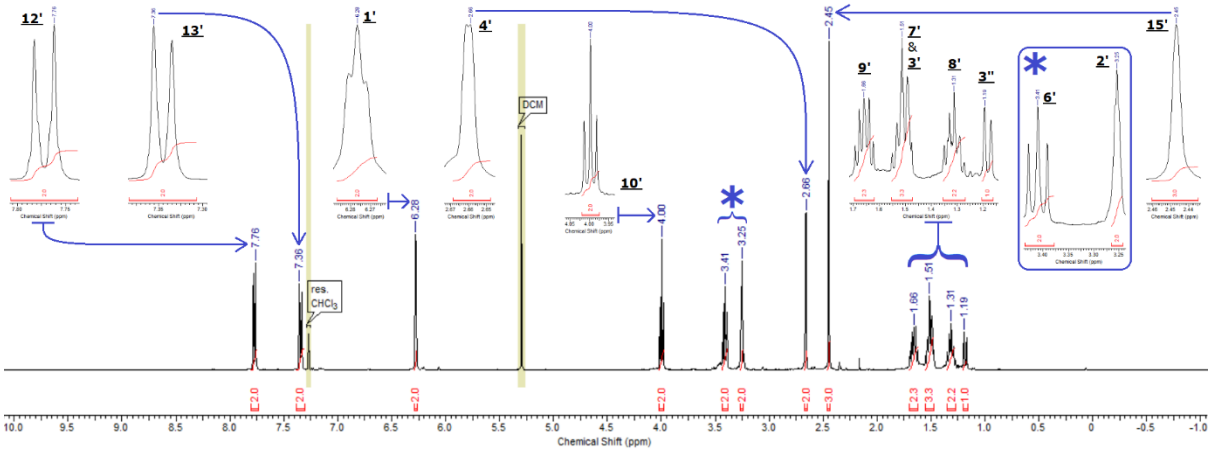

Figure 25: ^{1}H NMR of N-(5-tosylatopentyl)-*exo*-himide {***x*3**}.

NITRATION OF 2-AMINOBIPHENYL {ABP→4}

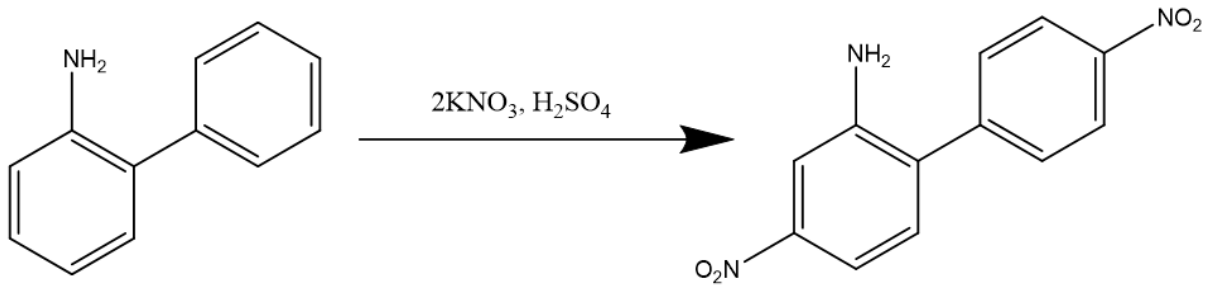

Figure 26: nitration of 2-aminobiphenyl {**ABP**} to 4,4'-dinitro-2-aminobiphenyl {**4**}.

2-aminobiphenyl (500 mg, 2.95 mmol) was dissolved in sulfuric acid (10 mL, 95%), then cooled to 0 C. Powdered sodium nitrate was added over the course of two hours, maintaining the temperature below 5 °C (see figure 26). After a further three hours, the reaction was slowly diluted with water and quenched with sodium hydroxide granules, reaching a slightly basic pH. The product was filtered and washed with water, dissolved in acetone and dried over magnesium sulfate before being crystallised in vacuo. The crude product (0.728 g, 95%) was recrystallised from acetone, yielding 4,4'-dinitro-2-aminobiphenyl (0.298 g, 39%); the mother liquor was retained as it contains most of the desired product.

Analysis of 4,4'-dinitro-2-aminobiphenyl {4}

M.P. decomposed 150–180 °C.

IR ν_{max}/cm^{-1}: 3462 (1° amine N–H ν_{as}, w); 3377 (1° amine N–H ν_{s}, w); 3105 (arene C–H ν, w); 3086 (arene C–H ν, w); 1630 (H–N–H δ, m); 1597 (arene C≈C β, m); 1503 (nitroarene N–O ν_{as}, s); 1339 (nitroarene N–O ν_{s}, s); 1279 (aniline C–N ν, s); 854 (arene C–H β, s); 814 (arene C–H β, s); 737 (1°/2° amine N–H ω, s). See figure 29.

^{1}H NMR (400 MHz, DMSO-d_6) δ/ppm: 8.33 (**24'**, 2H, dat, *J*=8.9, 2.5, 2.0 Hz); 7.75 (**23'**, 2H, dat, *J*=8.9, 2.5, 2.1 Hz); 7.65 (**17'**, 1H, d, *J*=2.4 Hz); 7.44 (**19'**, 1H, dd, *J*=8.4, 2.4 Hz); 7.28 (**20'**, 1H, d, *J*=8.4 Hz); 5.76 (**16"**, 2H, bs). See figure 27 and figure 28.

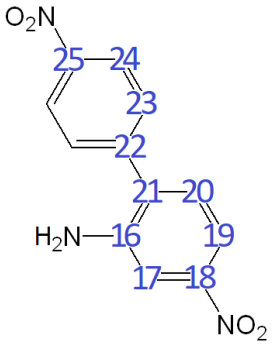

Figure 27: arbitrarily numbered structure of 4,4'-dinitro-2-aminobiphenyl {**4**}.

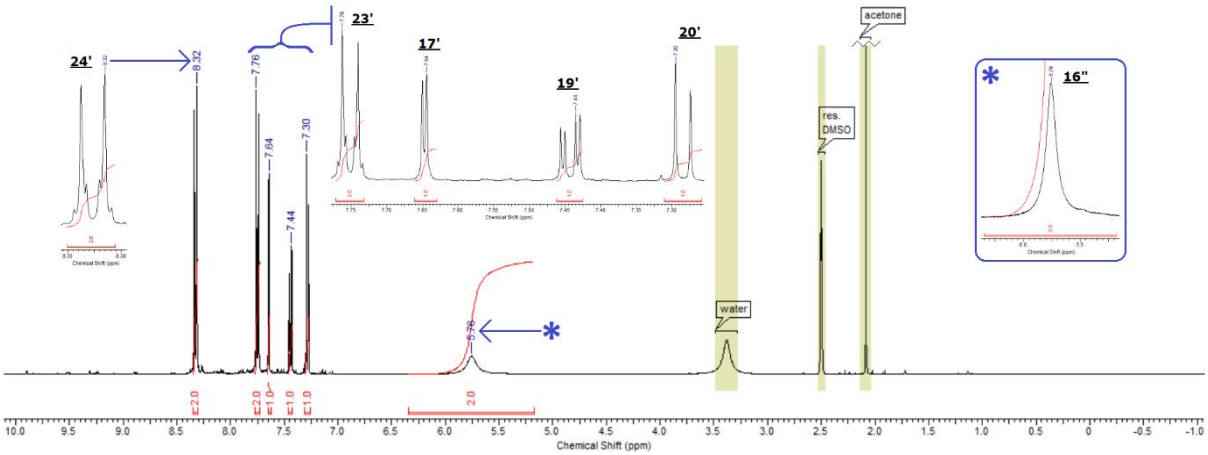

Figure 28: ^{1}H NMR of 4,4'-dinitro-2-aminobiphenyl {**4**}.

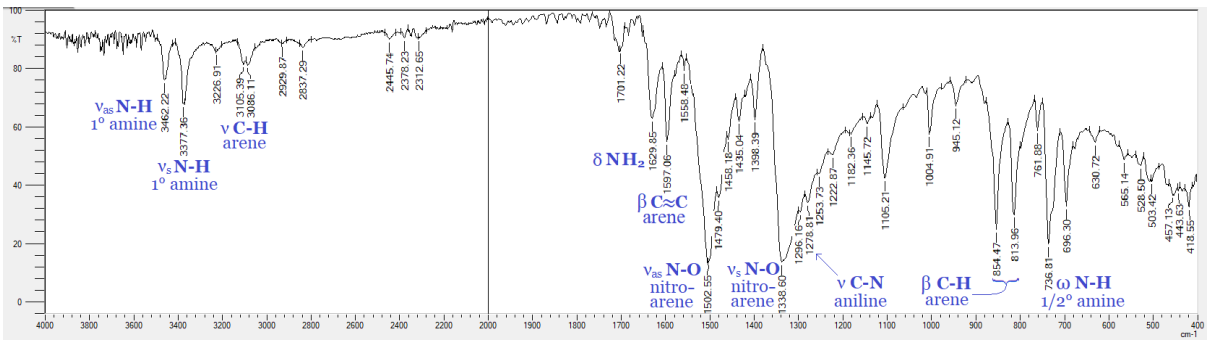

Figure 29: FT-IR of 4,4'-dinitro-2-aminobiphenyl {**4**}.

BENZCYCLIZATIONS {4→5} & {7→8}

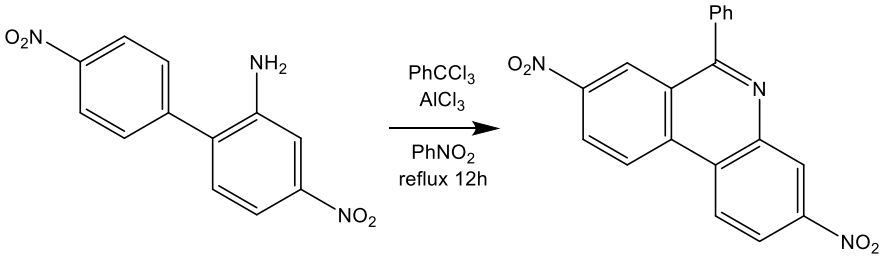

Figure 30: benzcyclization of 4,4'-dinitro-2-aminobiphenyl {**4**} to the phenanthridine {**5p**}.

A solution of 4,4'-dinitro-2-aminobiphenyl {**4**} (500 mg, 1.93 mmol) in nitromethane (20 mL) was heated under reflux with vigorous stirring, in an atmosphere of nitrogen, during the slow addition of benzotrichloride (2.75 mL, 19.4 mmol) and then aluminium chloride (50 mg, 0.37 mmol). After one hour, TLC indicated the complete conversion of the amine into a single product. Excess reactant was quenched with water (5 mL) and after five minutes the reaction mixture was concentrated *in vacuo*, dissolved in ethyl acetate (20 mL) and washed twice with water (2×20 mL), then dried over magnesium sulfate and again concentrated *in vacuo*. The resulting solid was washed with cold acetone (5 mL) to give a very pale yellow powder of *N*-(4,4'-dinitrobiphenyl-2-yl)benziminium dichloride {**5i**}. Further reaction under reflux in nitrobenzene for twelve hours (all other reagents, conditions and workup the same, see figure 30) yielded 3,8-dinitro-6-phenylphenanthridine {**5p**}.

Analysis of iminium chloride {5i}

M.P. 237–241 °C (with N deprotonated), 234–237 °C (salt with N protonated).

^{1}H NMR (400 MHz, DMSO-d_6) δ/ppm: 10.42 (**16"**, 1H, s); 8.46 (**17'**, 1H, d, *J*=2.4 Hz); 8.28 (**24'**, 2H, dat, *J*=8.9, 2.5, 2.0 Hz); 8.23 (**19'**, 1H, dd, *J*=8.6, 2.4 Hz); 7.79 (**30'**, **23'**, 4H, m); 7.74 (**20'**, 1H, d, *J*=8.6 Hz); 7.57 (**32'**, 1H, tt, *J*=7.3, 1.3 Hz); 7.48 (**31'**, 2H, ct, *J*=7.2 Hz). See figure 31 and figure 32.

^{13}C NMR: see figure 33 and figure 34.

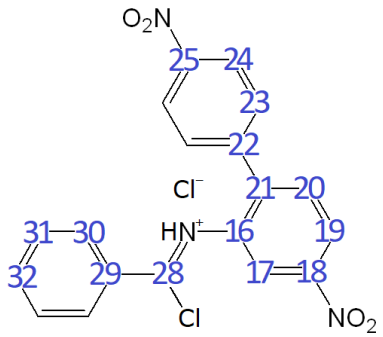

Figure 31: arbitrarily numbered structure of iminium chloride salt {**5i**}.

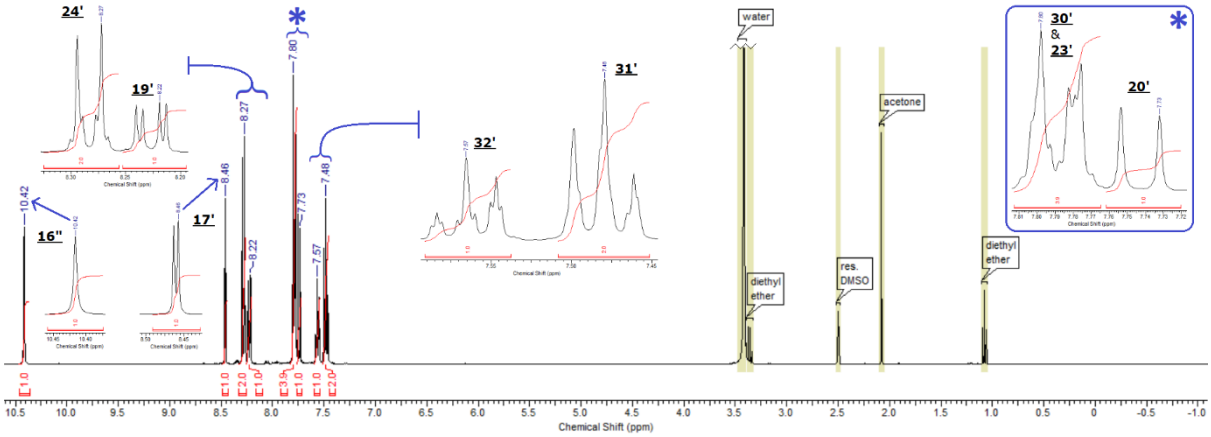

Figure 32: ^{1}H NMR of iminium chloride salt {**5i**}.

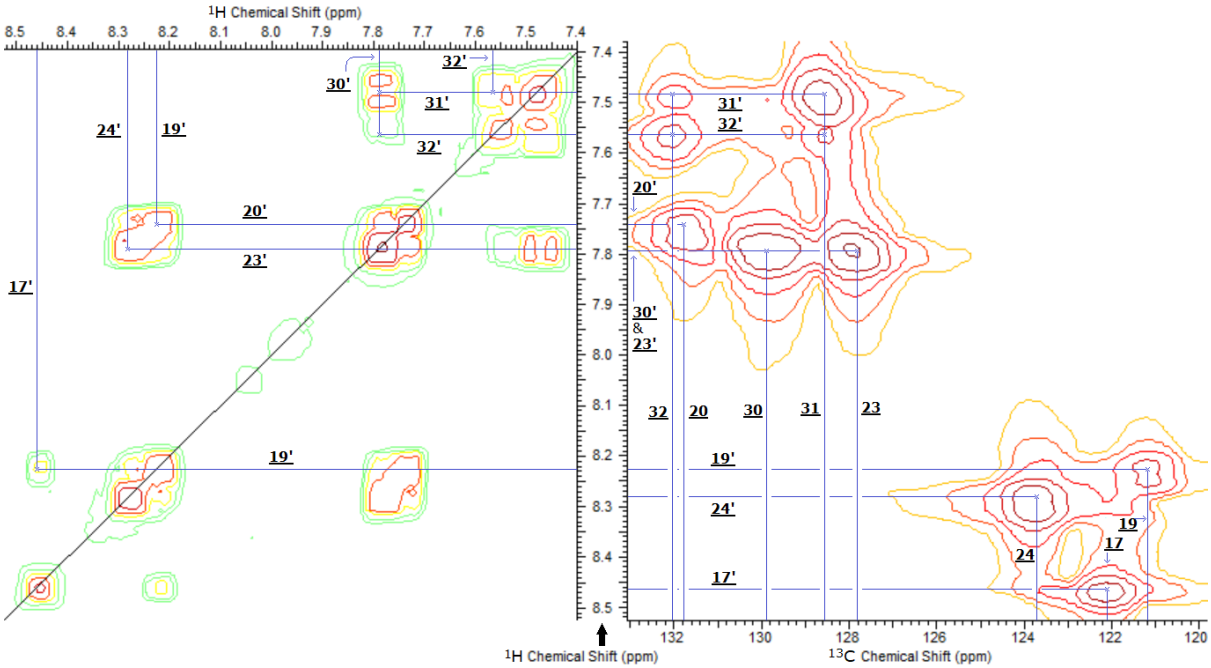

Figure 33: ^{1}H–^{1}H COSY (left) and ^{1}H–^{13}C HMQC (right) NMR of iminium chloride salt {**5i**}.

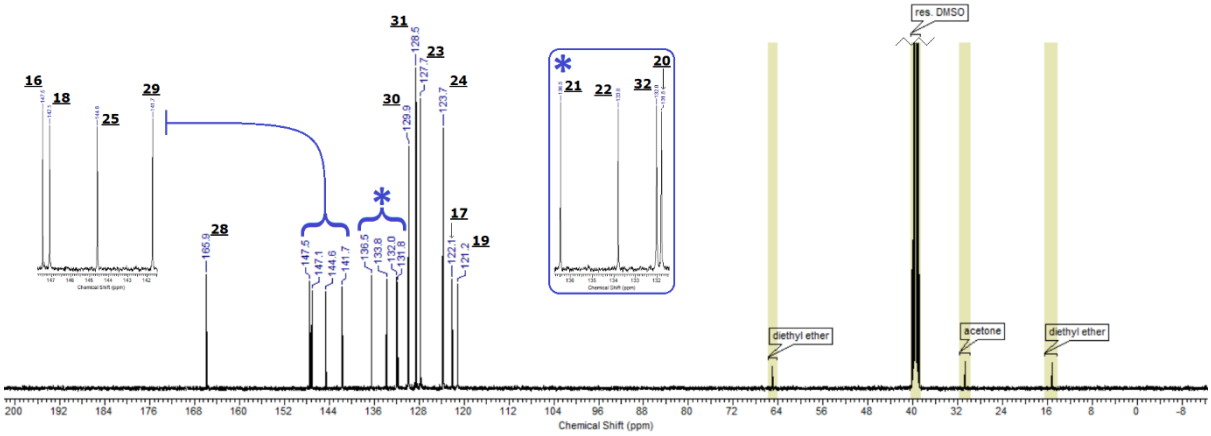

Figure 34: ^{13}C NMR of iminium chloride salt {**5i**}.

Analysis of 3,8-dinitro-6-phenylphenanthridine {5p}

^{1}H NMR (400 MHz, $CDCl_3$) δ/ppm: 9.18 (**23'**, 1H, d, *J*=2.4 Hz); 9.14 (**20'**, 1H, d, *J*=2.3 Hz); 8.93 (**17'**, 1H, d, *J*=9.0 Hz); 8.82 (**26'**, 1H, d, *J*=9.1 Hz); 8.76 (**19'**, 1H, dd, *J*=9.0, 2.3 Hz); 8.57 (**24'**, 1H, dd, *J*=9.0, 2.4 Hz), 7.80 (**31'**, 2H, m); 7.68 (**30'**, **32'**, 3H, m). See figure 35 and figure 36.

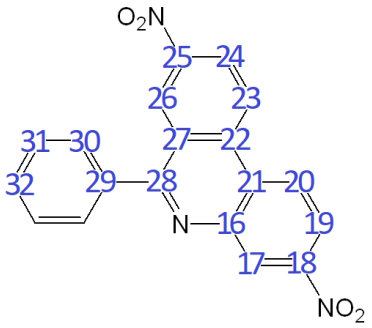

Figure 35: arbitrarily numbered structure of the phenanthridine {**5p**}.

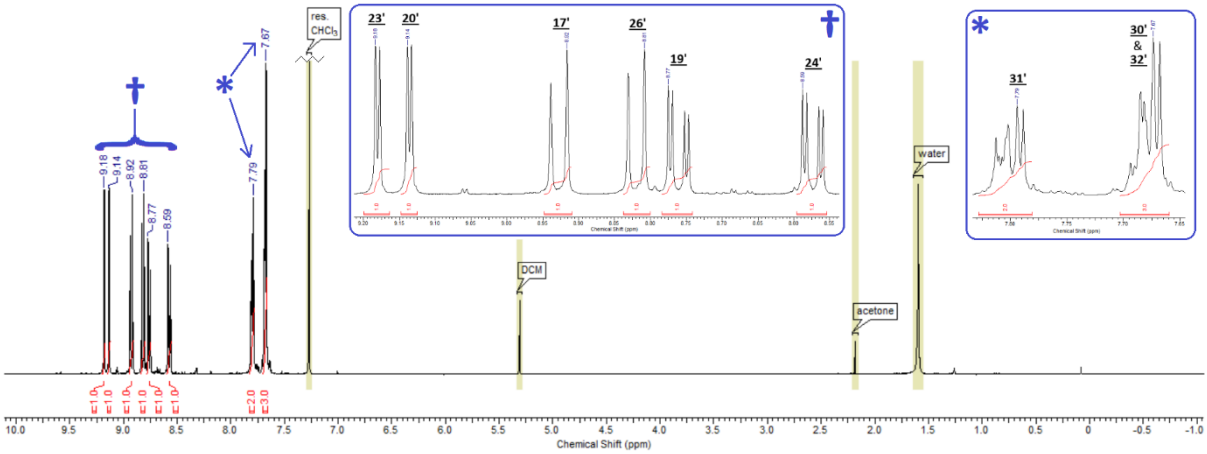

Figure 36: ^{1}H NMR of the phenanthridine {**5p**}.

Analysis: N-(5-(3,8-dinitro-6-phenylphenanthridinyl)-pentyl)-HimCl {8}

LC-MS (MeOH .3–.9, 20 min) m/z: 578 (M^+, 10.175 min, probe 650 °C, cone 200 V); 614 (HCl M^+, 10.392 min, probe 400 °C, cone 0.5 V). See figure 37, figure 38 and figure 39.

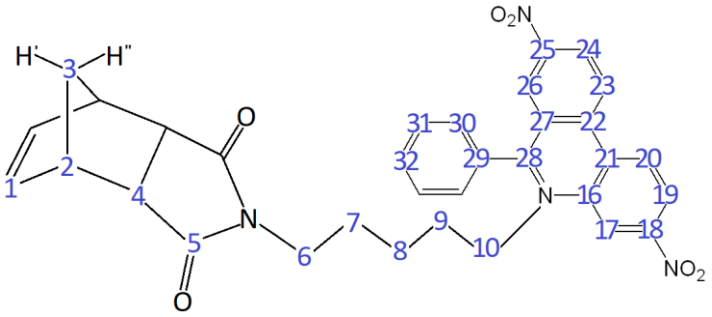

Figure 37: arbitrarily numbered structure of the dinitro-himidium compound {**8**}.

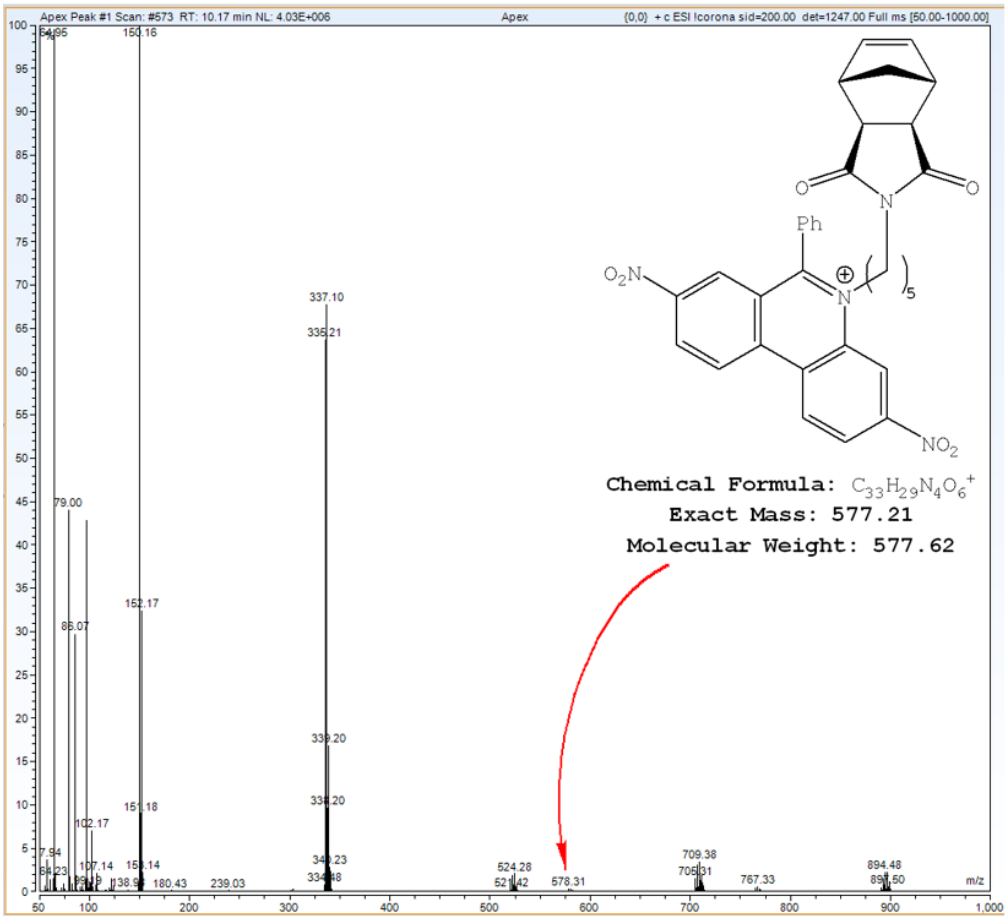

Figure 38: LC-MS of the dinitro-phenanthridine-himidium compound {**8**}.

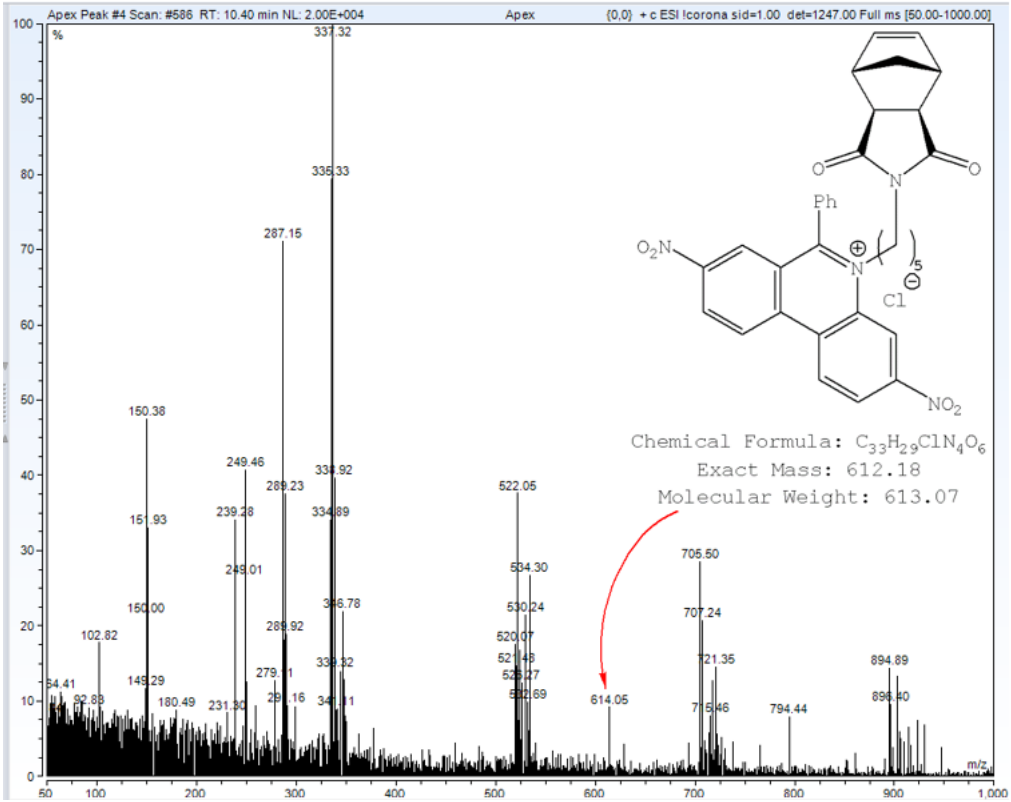

Figure 39: LC-MS of the HCl salt of the dinitro-phenanthridine-himidium compound {**8**}.

RESULTS & DISCUSSION

ISOMERISATION OF HIMIC ANHYDRIDE {***n*1→*x*1}**

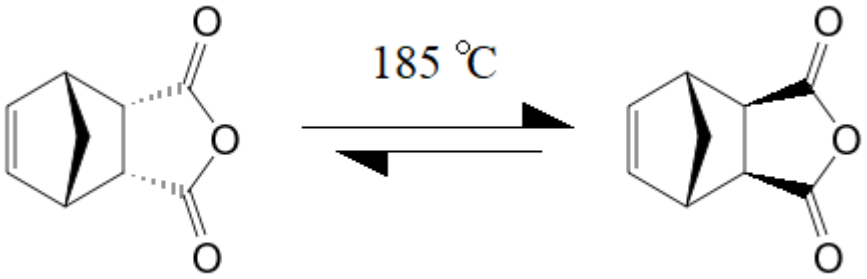

Figure 8: thermal isomerisation of *endo*-himic anhydride {***n*1**} to *exo*-himic anhydride {***x*1**}.

Himic anhydride and derivatives thereof exhibit *endo-exo* isomerism; the *endo* diastereomer polymerises less favourably due to steric clashes, so the desired *exo* must be isolated. *Endo*-himic anhydride {***n*1**}—which is very much cheaper to purchase than *exo* {***x*1**}—incompletely isomerises in the liquid phase by heating at 185 °C for several hours (see figure 8). Colleagues have in the past selectively recrystallised the desired isomer from boiling-hot toluene.[15] However, the reaction and work-up are deceptively tricky for several reasons.

First, himic anhydride undergoes a kind of sublimation that is analogous to evaporation: solid on the surface enters the gas phase without becoming liquid, at a pressure higher than its triple point. This vapour may then deposit on any colder surface of the vessel, often obscuring visibility, or be lost to the environment. For this reason, it is desirable to reach the melting point quickly: the liquid evaporates slower, perhaps due to its lower surface area. However, heating too quickly may cause localised overheating which can easily result in decomposition.

Second, the recrystallisation is very challenging: the boiling-hot toluene solution must be very slowly, passively cooled without moving the container (which must not be scratched) or introducing any other nucleation site, such as a stir rod. The minimum amount (estimated 2:1 ratio) of boiling toluene that will dissolve all of the solid should be used: too much and it won't recrystallise, not quite enough and the undissolved solids introduce nucleation sites.

Third, the isomerisation does not go to completion: the extent of reaction is just over 50% at best. The other half of the material is unrecoverable because the presence of residual toluene will preclude further isomerisation. This limits the theoretical yield to 50%, so it is important to not lose too much of it in recrystallisation. The

recrystallisation is very inefficient too: not only does much of the desired material remain in the mother liquor, but the crystals that do form are quite impure. Three consecutive recrystallizations are required to reach 98% purity, so in this reaction an overall yield of 11% is good.

The most characteristic ^{1}H NMR peak of the norbornene moiety throughout this work is the one slightly above 6 ppm, corresponding to the alkenyl proton. Because the alkene is chemically unaffected during the synthesis (until the polymerisation at the end), this peak was a useful starting point when interpreting the NMR spectra of norbornene derivatives. During some of the latter reactions, it was also useful for quickly checking that the temperature had not risen too high—which could potentially cause unwanted isomerisation—because (after the linker is attached) the chemical shift does not change significantly during the synthesis and is noticeably different between the two diastereomers.

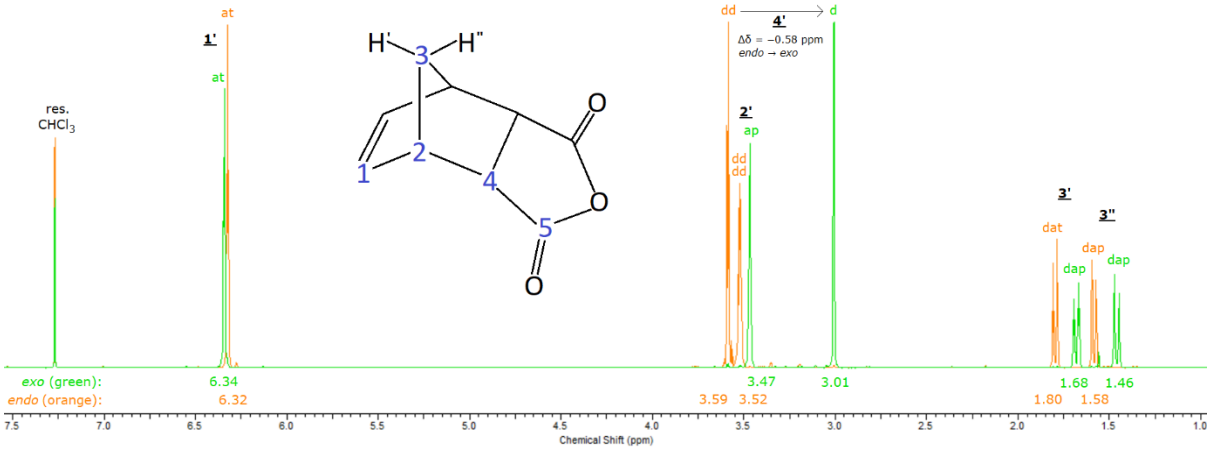

Figure 40: ^{1}H NMR comparison of the diastereomers of himic anhydride {**1**}.

1' produces an apparent triplet at 6.32 ppm in *endo*-himic anhydride and at 6.34 ppm in *exo*-himic anhydride. This is by far the most downfield peak in both spectra, due to the de-shielding effect of the π-bond in alkenes. It appears as a triplet, even though **1'** actually couples to two protons that are in *different* environments, because the two coupling constants are almost identical (J = 1.7 Hz for both, to 1 decimal place). Were the constants significantly different from one another, the peak would be a doublet of doublets instead. The protons to which **1'** couples must be: **2'** because they are vicinal—that is, in a 1,2-relationship—and **3"** due to a type of long-range coupling known as 'W-coupling'. See figure 40.

W-coupling is unusual in that it arises in saturated compounds: long-range coupling usually requires π-bonds. Coupling is not normally seen between atoms that are separated by four (or more) σ-bonds, but the methylene bridge of norbornene prevents ring inversion and forces the six-carbon ring to maintain a strained 'boat'

conformation. Therefore, the bonds between the two aforementioned coupled protons: **1'**–**1**–**2**–**3**–**3"** are locked in the shape of the letter 'W'. This configuration allows the anti-bonding orbitals of the two C–H bonds to overlap somewhat, which causes coupling between these structurally distant—but spatially proximate—protons.

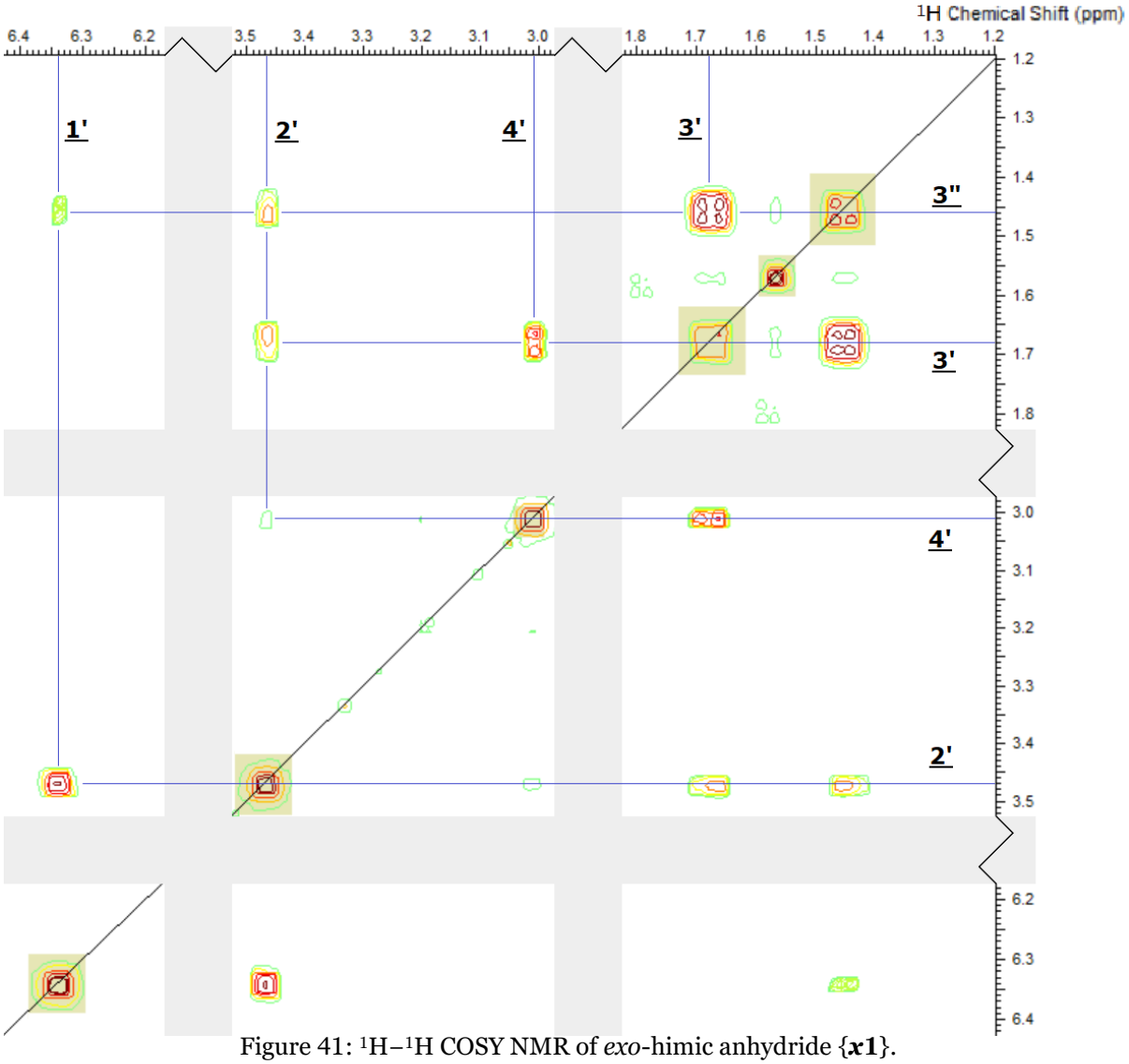

Figure 41: ^{1}H–^{1}H COSY NMR of *exo*-himic anhydride {***x*1**}.

According to the COSY (see figure 41), **1'** couples to an apparent pentet at 3.47 ppm and to a doublet of apparent pentets at 1.46 ppm. The alkene is expected to de-shield the vicinal proton more than the one on the bridge (due to closer proximity); thus, the former peak is assigned to **2'** and the latter to **3"**. These assignments are also supported by the splitting patterns: the bridgehead proton couples to its four vicinal neighbours (both bridge protons, the alkenyl proton and the proton on the ring fusion carbon) so **2'** appears as a pentet. This implies that the coupling constants must all be quite similar, otherwise it would be a doublet of doublets of doublets of doublets, like it is in the *endo* spectra.

Meanwhile, **3"** couples very strongly with its geminal neighbour (the other bridge proton, J = 10.2 Hz), but far more weakly with the pair of vicinal bridgehead protons and with the pair of hominal (that is, in a 1,3-relationship) alkenyl protons (the latter due to W-coupling). The two smaller constants must be very similar because **3"** appears as a doublet of pentets (otherwise it would be a doublet of triplets of triplets). The COSY evinces additional couplings of these newly-assigned peaks: of **3"** to 1.68 ppm and of **2'** to 1.68 ppm and 3.01 ppm. The only other proton to which *both* of these may be coupling is **3'**, so that is the assignment of the peak at 1.68 ppm; by process of elimination, then, 3.01 ppm is assigned as **4'**.

The splitting pattern of **3'** is essentially the same as that of the other bridge proton: a doublet of apparent pentets, although in this case the long-range coupling is to **4'**, because they form the 'W' shape in the *exo*-diastereomer. By contrast, W-coupling is not possible between these two protons in the *endo* compounds because **4'** is pointing in the wrong direction, so **3'** appears as a doublet of triplets (rather than a doublet of pentets). Meanwhile, the orientation of **1'** is not significantly affected by the isomerisation, so it does couple to **3"**, which therefore appears as a doublet of pentets in the *endo* spectrum.

4' couples to its vicinal neighbour **2'** in both diastereomers, but the intensity of that coupling (as indicated in the COSY) is quite different between the two: in the *exo* diastereomer, it is surprisingly weak. In fact, it is much weaker than the coupling between **4'** and **3'**. Therefore, the peak that corresponds to **4'** is split into a doublet by long-range coupling (in a saturated moiety, no less), while the vicinal coupling—which one might, at first glance, presume to be responsible for creating the doublet—is actually so weak that the peak shows no visible sign of second-order complexity. This is due to the dihedral angle being close to 90°, as per the Karplus equation.

The Biagini group observed the **4'** peak in *endo*-himic anhydride to be a quartet, despite the COSY not showing any coupling to that proton except by **2'**, which one "would expect to result in a triplet". It was explained that this discrepancy "hasn't been fully understood but is likely the result of long-range coupling within the norbornene that is not entirely obvious".[15] The identity of this coupling can now be suggested: the bonds between **4'** and **1'** may be close enough to the required shape for weak W-coupling between them in the *endo*-diastereomer, but not in the *exo*-compounds. This could also explain why **4'** is significantly (about 0.57 ppm) further downfield in the latter than in the former.

IMIDIZATION OF HIMIC ANHYDRIDE {1→2}

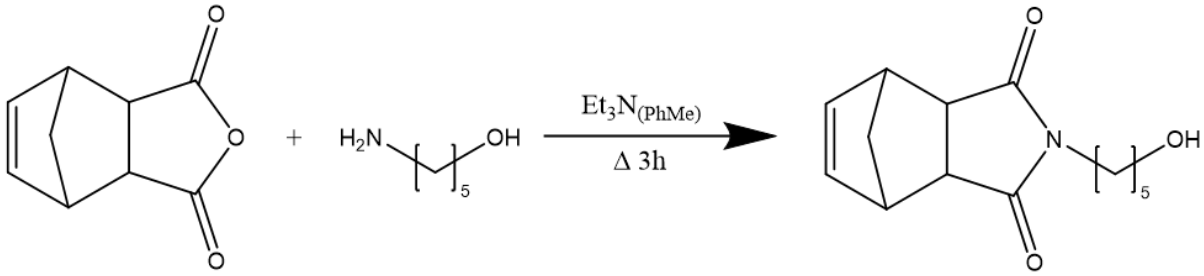

Figure 12: himic anhydride {**1**} reacts with 5-aminopentanol {**AP**} to form a himidol {**2**}.

As explained previously, in the discussion of the isomerisation {***n*1→*x*1**}, the peak of the alkenyl proton **1'** is generally unchanged from one reaction to the next: it remains an apparent triplet just above 6 ppm throughout. However, the exception is that its chemical shift changes slightly during the imidization {**1→2**}: it is moved upfield (see figure 42). This is unlikely to be due to the change of functional group, as the new nitrogen atom is five σ-bonds away from the alkenyl proton (see figure 12). The difference is four times larger for the *endo* than the *exo*: $\Delta\delta_{1'}${***n*1→*n*2**} = −0.24 ppm while $\Delta\delta_{1'}${***x*1→*x*2**} = −0.06 ppm. This suggests that this upfield shift may be due to a direct interaction between the alkene and a part of the linker—apparently the hydroxyl oxygen atom—because the two ends of the molecule are able to get close together much more easily in the *endo* compounds than in the *exo* ones.

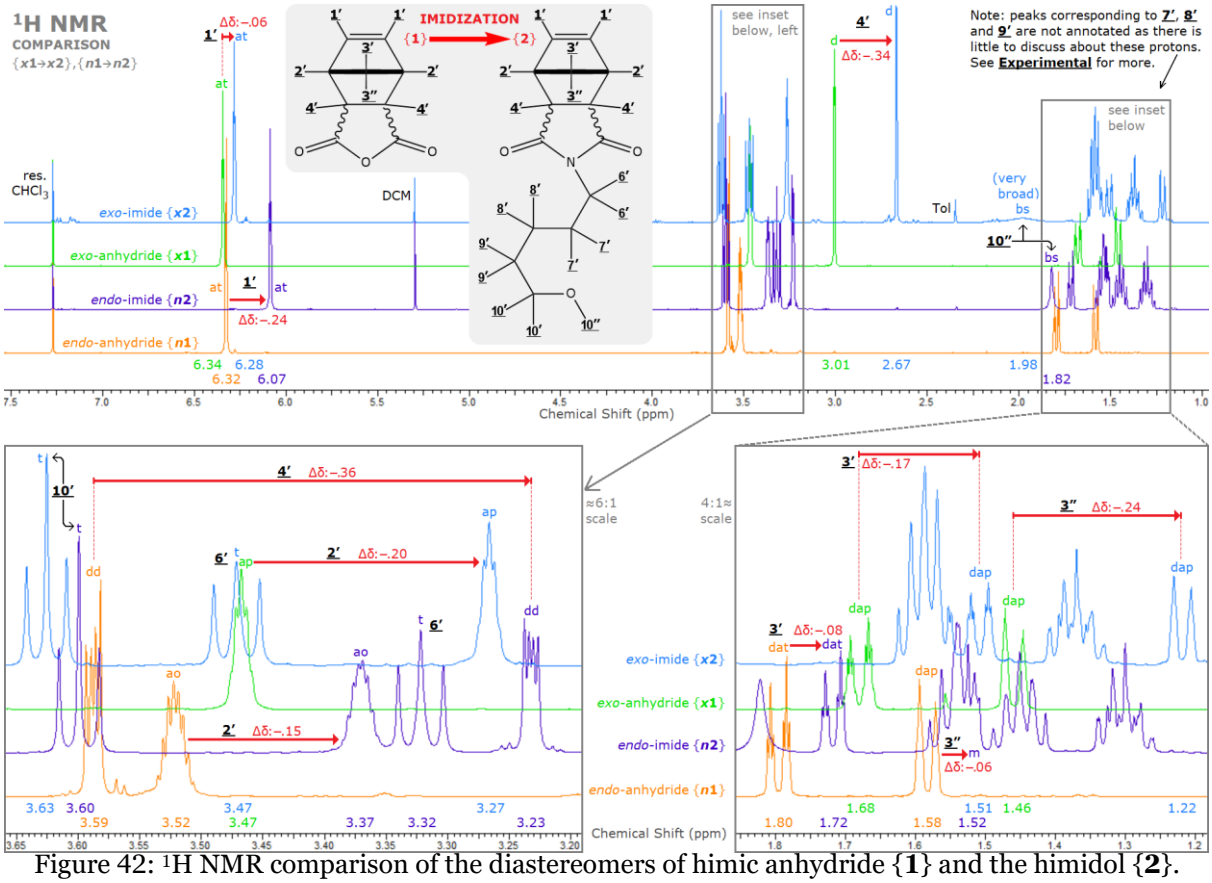

Figure 42: ¹H NMR comparison of the diastereomers of himic anhydride {**1**} and the himidol {**2**}.

That an intramolecular interaction between opposite ends of the *endo*-himidol {***n*2**} may be responsible for the change in chemical shift of the alkenyl proton **1'** may be corroborated by comparing the hydroxyl oxygen **10"** peaks of the two diastereomers. Both are broad singlets, but that of the *exo*-himidol {***x*2**} is very much the broader (so diffuse that it is scarcely visible above the baseline), while its chemical shift is further downfield: $\delta_{\mathbf{10"}}\{\boldsymbol{x}\mathbf{2}\}$ = 1.98 ppm versus $\delta_{\mathbf{10"}}\{\boldsymbol{n}\mathbf{2}\}$ = 1.82 ppm. This might be dismissed as simply an artefact of water impurity in the sample causing hydrogen bonding, but if that were so, then the relative integral of this peak would be larger: it is exactly 1H (reckoned with low precision but good accuracy) for both diastereomers. If the hydroxyl group of *endo*-himidol is shielding the *cis*-vinylene group by dipole-dipole interactions, then it is plausible that this hydroxyl group is engaged less frequently (in *endo* than *exo*) in similar interactions with the imide group. This would explain why **10"** (which can't interact significantly with the vinylene) is further downfield and much broader: signs of greater hydrogen bonding with the five lone pairs of the imide group, coloured blue in Figure 43.

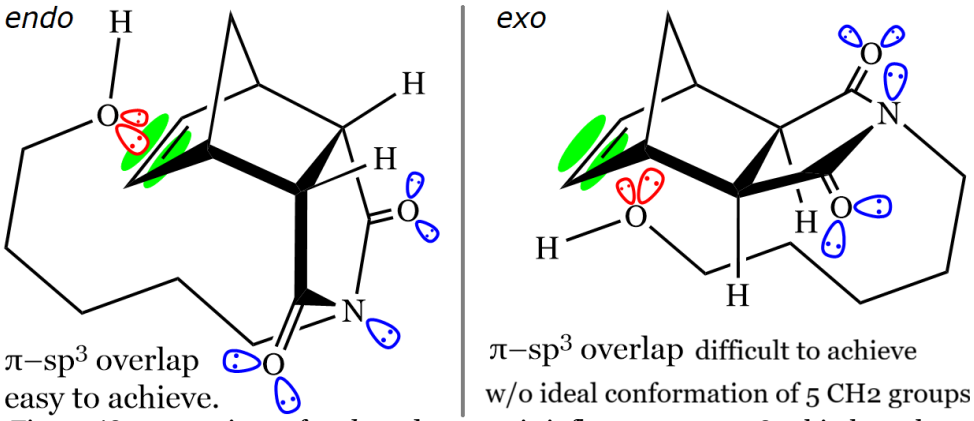

Figure 43: comparison of *endo* and *exo* steric influence on π–sp3 orbital overlap.

These subtle differences between the NMR spectra of the two diastereomers hint at the reason why care had to be taken to isolate *exo*-himic anhydride and to ensure that isomeric purity was preserved throughout the synthesis. It has been known for decades that ROMP of *N*-substituted himides proceeds at different rates and can yield somewhat variable polymers depending on the diastereomeric composition of the monomer used. In 1998, Biagini et al.[11] reported that "the *endo* monomers polymerise appreciably slower than their *exo* counterparts … most likely a consequence of unfavourable steric interactions between the [*N*-substituent] group in the *endo* isomer and … the initiator." The group in question was only five bonds long, N-to-end, compared to seven in the present work; the longer it is, the closer it can get to the site where it causes problems. If the *endo* vinylene (which is the reactive centre in ROMP) is interacting with the linker as evidenced above, this presupposes that the opposite ends of the molecule are often in close proximity; therefore, polymerisation of *endo*-himidium chloride would probably be significantly sterically hindered.

Unsurprisingly, the ring fusion/junction protons **4'** experienced the largest change in chemical shift of the five norbornene proton environments present: $\Delta\delta_{4'}\{\boldsymbol{n1}\rightarrow\boldsymbol{n2}\}$ = −0.36 ppm and $\Delta\delta_{4'}\{\boldsymbol{x1}\rightarrow\boldsymbol{x2}\}$ = −0.34 ppm. There is almost no difference (0.02 ppm) between the two values because these protons are on the ring that contains the imide, so their orientation relative to the imide group is essentially the same for *endo* and *exo* (see Figure 42). The magnitude of the change is so large because they are the closest protons to the imide group, which is a significantly less electron-withdrawing group than anhydride. This is due to the nitrogen atom causing resonance stabilisation by donating electron density toward the carbonyls, which also makes imides less susceptible to nucleophilic attack than anhydrides. Similarly, the bridgehead protons **2'** are shifted upfield significantly—but less than **4'** because they are further from the imide group—and by approximately the same amount for both diastereomers: $\Delta\delta_{2'}\{\boldsymbol{n1}\rightarrow\boldsymbol{n2}\}$ = −0.15 ppm and $\Delta\delta_{2'}\{\boldsymbol{x1}\rightarrow\boldsymbol{x2}\}$ = −0.20 ppm.

The bridge protons **3'** and **3"** also undergo an upfield change in chemical shift during the imidization, but its magnitude differs greatly between the two diastereomers. The change is small for the *endo*, and similar for both protons: $\Delta\delta_{3'}\{\boldsymbol{n1}\rightarrow\boldsymbol{n2}\}$ = −0.08 ppm and $\Delta\delta_{3"}\{\boldsymbol{n1}\rightarrow\boldsymbol{n2}\}$ = −0.06 ppm. This is in keeping with the trend (mentioned in the previous paragraph) of protons that are further away from the anhydride/imide ring being less affected by the change in functional group during the imidization $\{\boldsymbol{n1}\rightarrow\boldsymbol{n2}\}$: $\Delta\delta_{4'} > \Delta\delta_{2'} > \Delta\delta_{3'}$ & $\Delta\delta_{3"}$. However, this trend is broken by the *exo*, with the chemical shifts of both bridge protons (**3'** and **3"**) being affected more than those of their bridgehead (**2'**) neighbours. Additionally, the *syn* bridge proton **3"** is affected significantly more than the *anti* bridge proton **3'**. This aberration could be due to overlap of the C–N σ* antibonding orbital of the imide group with the C–H σ* antibonding orbitals of the bridge.

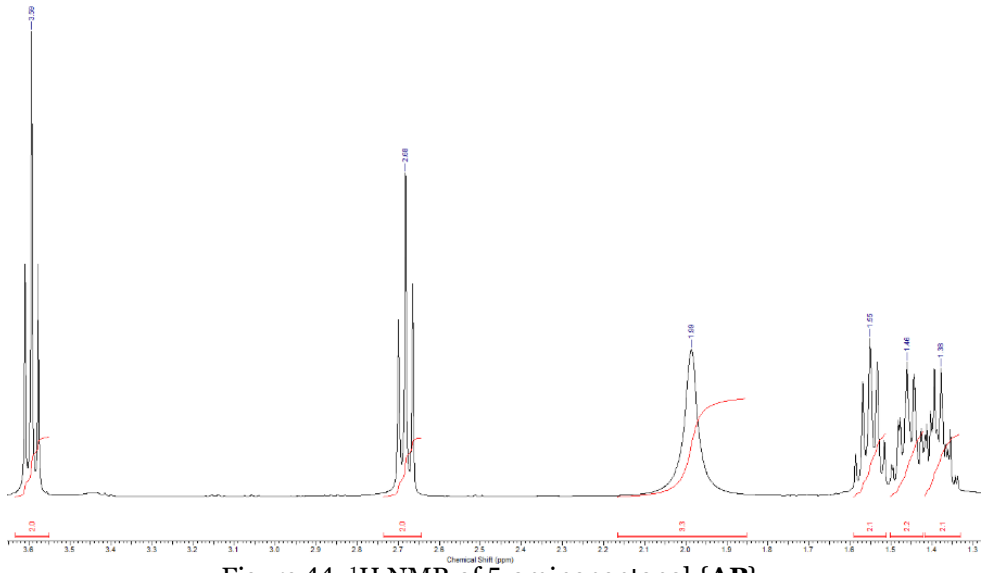

Figure 44: ^{1}H NMR of 5-aminopentanol {**AP**}.

Finally, the triplet corresponding to the linker proton **6'** that is closest to the imide group experiences the largest change in chemical shift overall. Compared to the starting material, 5-aminopentanol {**AP**}, *exo* is affected more than *endo*, but both are moved considerably: $\Delta\delta_{6'}${**AP**→***x*2**} = +0.79 ppm while $\Delta\delta_{6'}${**AP**→***n*2**} = +0.64 ppm (see figure 44). This is simply due to this methylene group being de-shielded more by the imide group than the amine, because, as mentioned earlier, the nitrogen atom of the imide donates electron density towards the carbonyls, which therefore makes this methylene more electron-withdrawn. Note also that the broad singlet of 5-aminopentanol {**AP**}, corresponding to OH and NH_2, has the same chemical shift (δ = 1.99 ppm) as that of the *exo*-himidol {***x*2**}; both would be expected to hydrogen bond with themselves freely, while the *endo* {***n*2**}, as suggested previously, is preoccupied with interacting with the vinylene, and has a smaller chemical shift.

The ^{1}H–^{1}H COSY NMR spectrum was helpful in assigning the ^{1}H NMR spectrum, but there is little of note to mention about it, so it is included here, in figure 45, for reference and completeness.

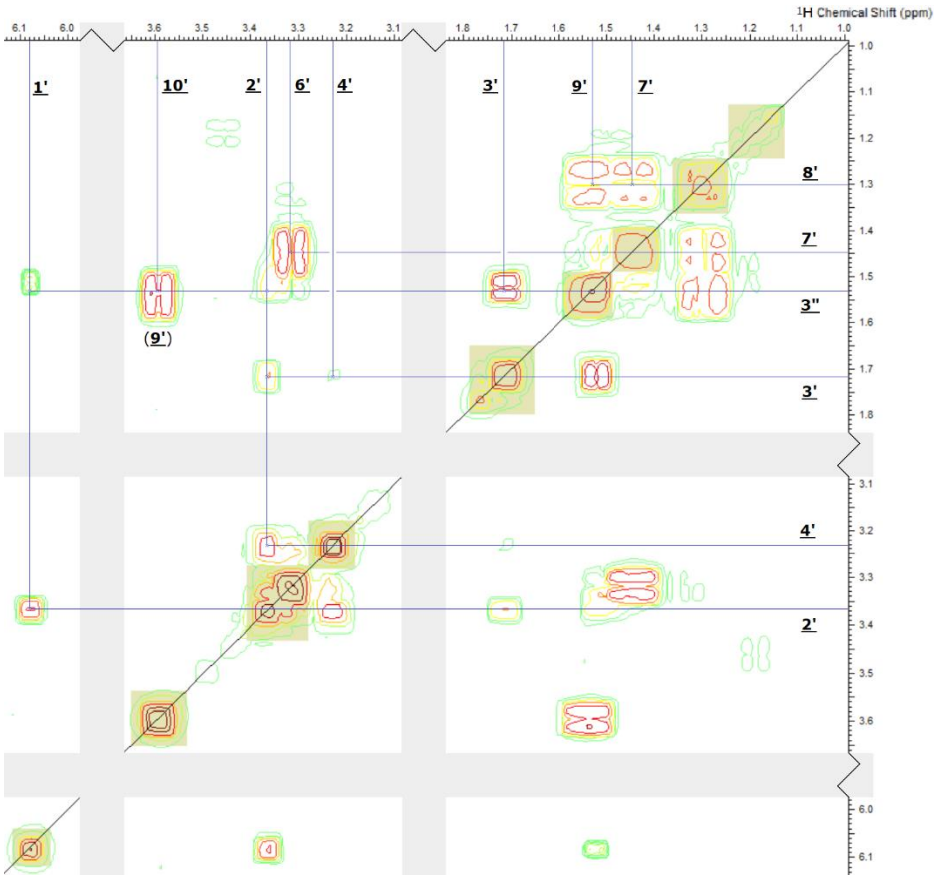

Figure 45: ^{1}H–^{1}H COSY NMR of N-(5-hydroxypentyl)-*endo*-himide {***n*2**}.

TOSYLATION OF HIMIDOL {2→3}

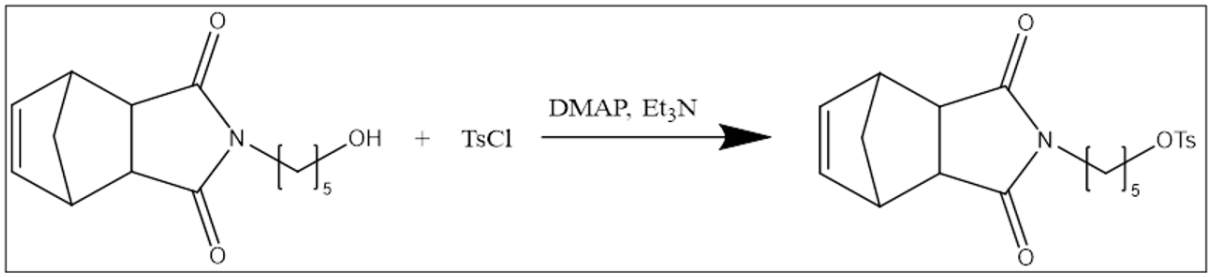

Figure 20: tosylation of himidol {**2**} to himide-tosylate {**3**}.

After an unsuccessful attempt using pyridine, the tosylation was successfully conducted with the more nucleophilic catalyst 4-dimethylaminopyridine (DMAP), as well as triethylamine, which acts as a proton acceptor to regenerate the catalyst (see figure 20 and figure 46).

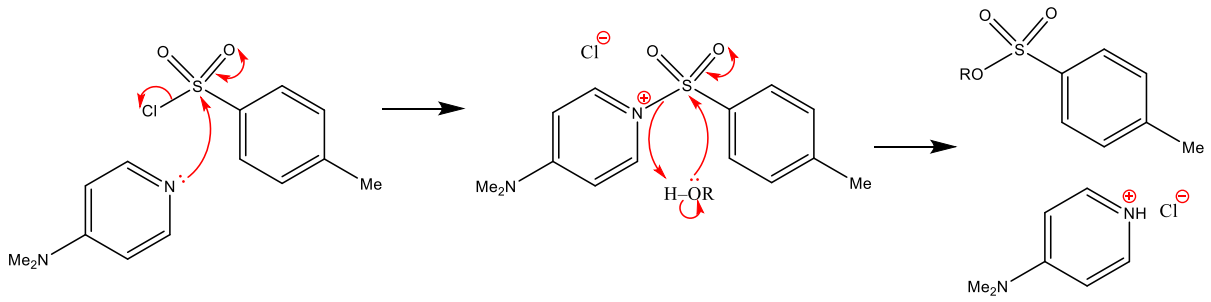

Figure 46: general tosylation mechanism.

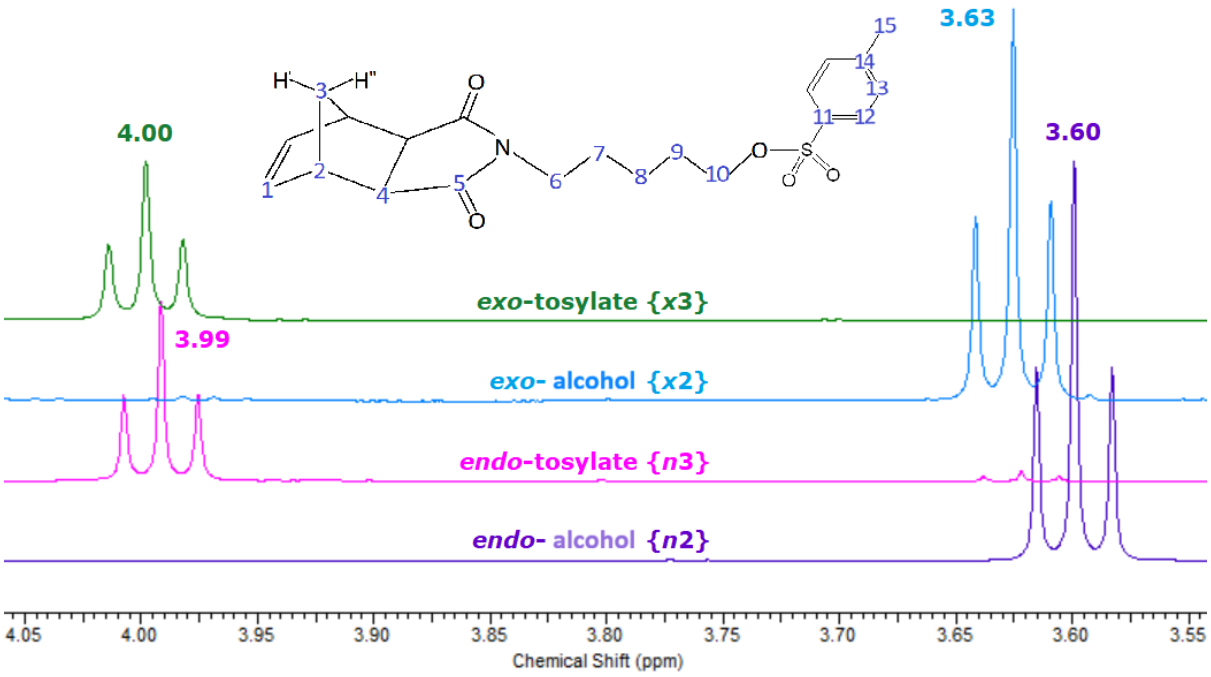

Figure 47: ^{1}H NMR comparison of **10'** for the diastereomers of the tosylate {**3**} and the himidol {**2**}.

The only ^{1}H NMR peak that moved significantly during the tosylation {**2**→**3**} is the triplet corresponding to the linker methylene protons **10'** that are furthest away from the imide group: $\Delta\delta_{10'}\{\boldsymbol{n2}\rightarrow\boldsymbol{n3}\}$ = +0.39 ppm and $\Delta\delta_{10'}\{\boldsymbol{x2}\rightarrow\boldsymbol{x3}\}$ = +0.37 ppm (see figure 47). This is because that methylene group is adjacent to the newly introduced *para*-toluenesulfonate ("tosylate") group, which is much more electron-withdrawing than hydroxyl. The same property also causes the TosO–CH_2 bond to be very polarised and easy to break, which is why tosylate is such a good leaving group.

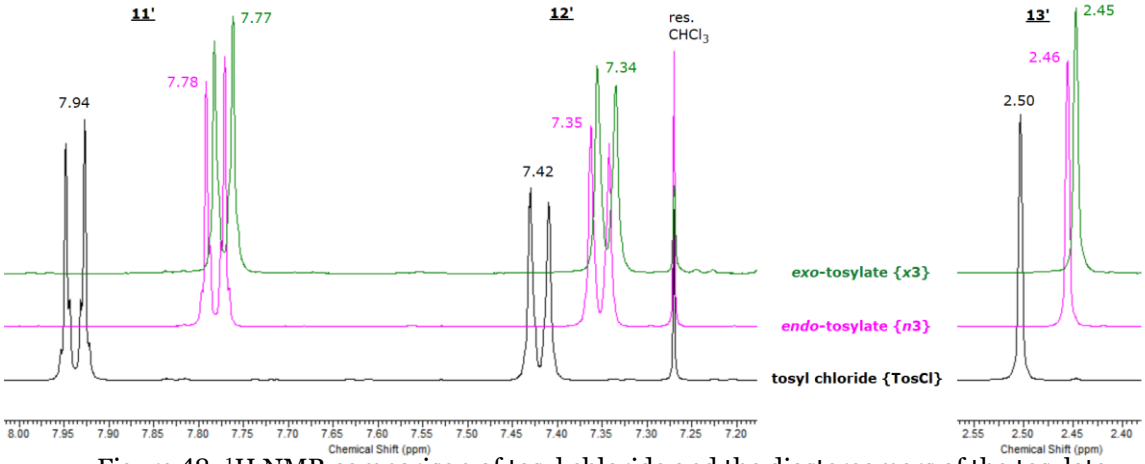

Figure 48: ^{1}H NMR comparison of tosyl chloride and the diastereomers of the tosylate.

The electron density that the tosylate withdraws from the linker also causes its tolyl group to become slightly more shielded, compared to the tosyl chloride reagent. Conversely, it could be said that the change is due to the removal of the electron-withdrawing chloride. The methyl group is a singlet, as expected, but the aromatic protons each appear as doublets of triplets: the doublet due to coupling with its vicinal neighbour, and the apparent triplet due to long-range coupling across the ring (see figure 48). None of the four protons is equivalent to any other, due to the asymmetric geometry of the tosylate group and the barrier to relative rotation around the sulfur-carbon bond (see figure 49).

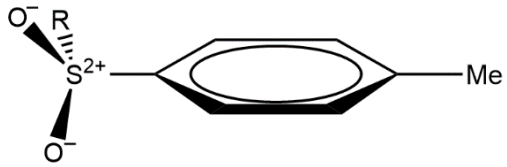

Figure 49: structure of the tosyl group; S=O shown as S–O$^-$ to better display the symmetry.

NITRATION OF 2-AMINOBIPHENYL {ABP→4}

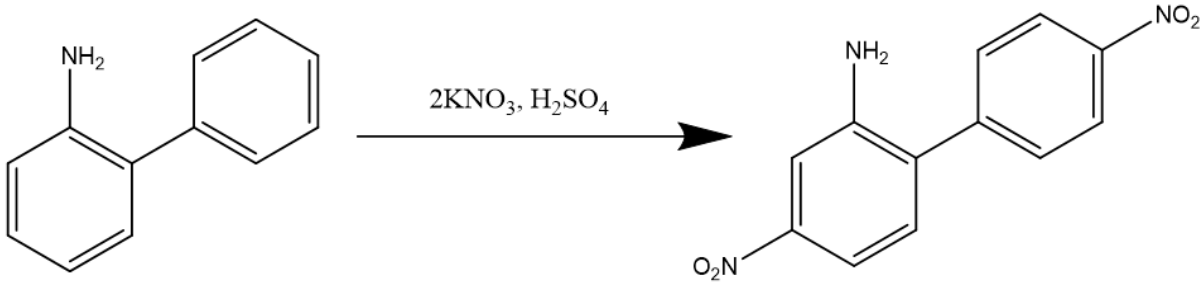

Figure 26: nitration of 2-aminobiphenyl {**ABP**} to 4,4'-dinitro-2-aminobiphenyl {**4**}.

Double nitration of 2-aminobiphenyl {**ABP**} was achieved at the positions *para* to the inter-ring bond with very high regioselectivity and relative ease, though care had to be taken to ensure that over-nitration did not occur, which could plausibly produce explosive side-products related to trinitrotoluene (TNT). The reaction was performed at 0±5 °C with constant stirring, and potassium nitrate (instead of the usual nitric acid) was added gradually over two hours; these measures were designed to slow the reaction rate and limit the production of unwanted side-products. For the same reason, only a stoichiometric quantity of the nitrate salt was used (see figure 26).

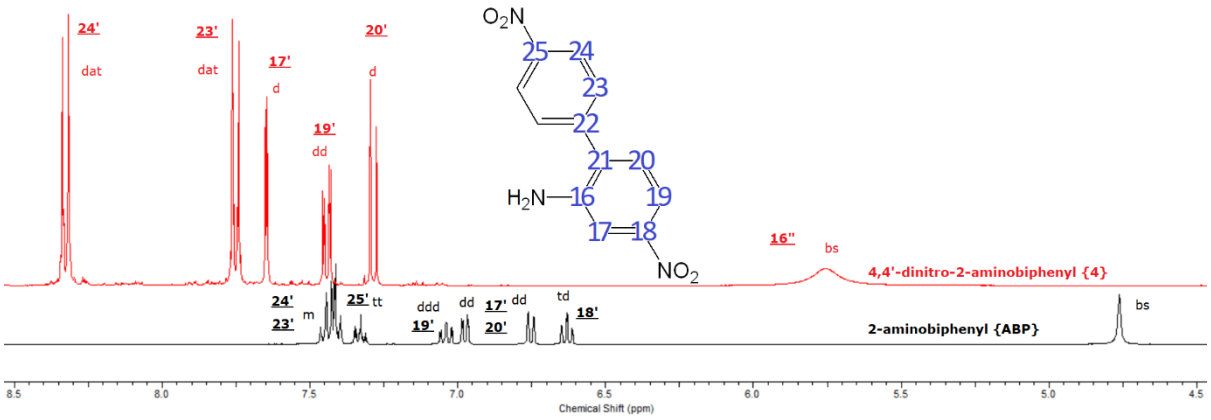

Figure 50: ^{1}H NMR comparison of 2-aminobiphenyl {**ABP**} and its 4,4'-dinitrate {**4**}.

The most noticeable effect of nitration on the ^{1}H NMR of these compounds is that in the spectrum of the product: 4,4'-dinitro-2-aminobiphenyl {**4**}, every peak is shifted significantly downfield compared to the starting material (figure 50). The protons of the amine **16"** are shifted a full 1 ppm downfield (despite NH_2 being *meta* to NO_2), indicating that a significant amount of the amine lone pair is donated to the ring, making it a worse nucleophile for further reactions. This would later cause difficulties for the benzcyclization reactions.

Each of proton pairs **23'** and **24'** on the nitrophenyl ring gives rise to a doublet of apparent triplets with a relative integral of 2H. The doublets are due to strong vicinal

coupling (^3J) between the two proton environments, while the apparent triplet is due to weak long-range couplings to the respective *meta* (^4J) and *para* (^5J) positions. Similarly to the tosylate in the previous section, there is a barrier to rotation around the inter-ring bond (due to repulsion between *ortho* protons); additionally, the lowest-energy torsion angle between the rings is oblique; for these reasons, the two protons in each pair (*meta* to each other) are effectively in slightly different environments.

Splitting patterns for those proton pairs in the starting material, 2-aminobiphenyl {**ABP**}, are difficult to determine because the two signals overlap. This coincidence is enabled by the absence of the nitro group—or any other substituent—on the phenyl ring, and the lack of shared aromaticity between the rings (which is explained below). By contrast, in the product {**4**}, protons **24'** are much further downfield than **23'** partly due to proximity to the strongly electron-withdrawing nitro group, but more importantly because resonance within the ring causes less deshielding of the positions *meta* to the nitro than of the *ortho* (and *para*). These are the most downfield peaks in the spectra of both compounds because the only difference between the two rings is the amino group, which donates electron density into the aniline ring, whose protons are thus shielded more, while **23'** and **24'** are not significantly affected, again due to the lack of inter-ring aromaticity.

On the nitroaniline ring, proton **19'** couples to its vicinal neighbour **20'**, and couples long-range to **17'**, but unlike the other ring, there is no evidence of ^5J coupling between *para* protons. Therefore, **19'** gives rise to a doublet of doublets, whereas the other two peaks are just doublets. No coupling is observed between the rings (eg. **20'** with **23'**) because the aforementioned torsion angle prevents overlap of the π systems, so the inter-ring bond is just a single σ bond.

BENZCYCLIZATION OF PRIMARY AMINE {4→5}

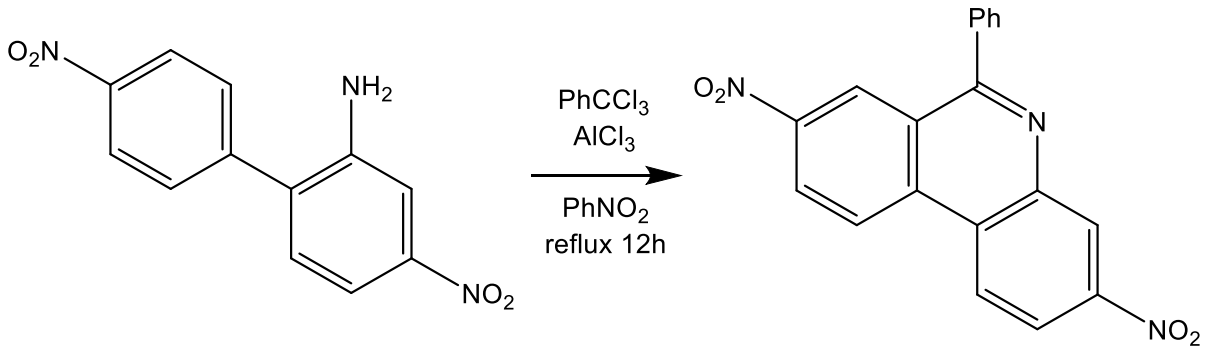

Figure 30: benzcyclization of 4,4'-dinitro-2-aminobiphenyl {**4**} to the phenanthridine {**5p**}.

Initially, benzcyclization of the primary amine 4,4'-dinitro-2-aminobiphenyl {**4**} was attempted in nitromethane solvent because it is much less toxic than nitrobenzene, which is usually used in the literature.[18] However, the boiling point of nitromethane is 101 °C, which proved inadequate for the Friedel-Crafts, but the N-substitution did occur, yielding an iminium chloride salt {**5i**}. The high activation energy barrier of the Friedel-Crafts can be attributed to the strongly deactivating effect of nitro-groups on SEAr. The energy barrier is even higher for further alkylation, which would not benefit from the stabilization of forming an aromatic ring or from the enhanced electrophilicity of iminium chlorides, hence over-alkylation is strongly inhibited and was not observed.

The reaction was repeated on the same primary amine {**4**} under reflux with nitrobenzene as solvent, yielding the desired phenanthridine {**5p**} (see figure 30). These more aggressive conditions were then applied to the iminium chloride {**5i**}, confirming that it was an intermediate in forming the phenanthridine {**5p**} (see figure 51), and on a secondary amine, which yielded a phenanthridinium (see Figure 54).

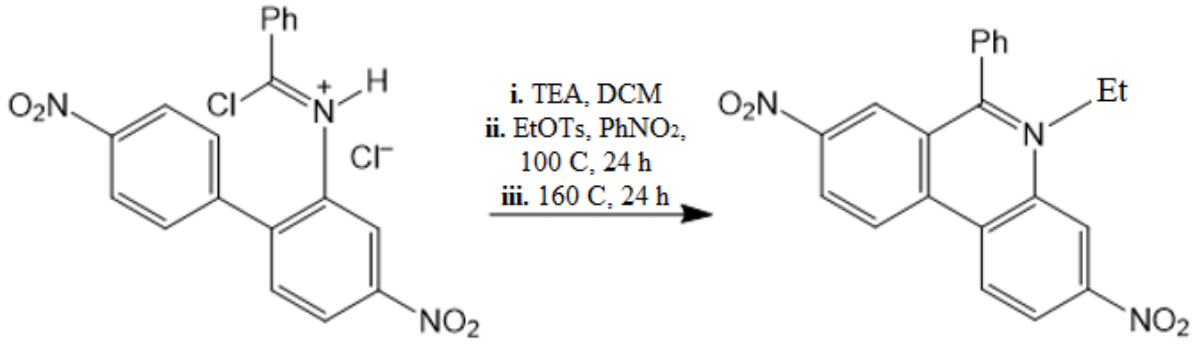

Figure 51: iminium chloride {**5i**} is an intermediate in producing the phenanthridine {**5p**}.

The phenanthridine {**5p**} was very resistant to later coupling to the norbornene-linker adduct, so towards the end of the project the order of reactions was reversed, as discussed in the next chapter, with the coupling happening before benzcyclization. This meant that benzcyclization had to be performed at a much lower temperature (160 °C) in order to not degrade the norbornene, and that the nitrogen centre would be less nucleophilic due to the alkyl linker while also being slightly more sterically hindered. Nonetheless, the reaction was successful, likely indicating that neither of the benzcyclization reactions requires a temperature as high as 211 °C, but only 160 °C.

Assignment of the ^{1}H NMR spectrum of 3,8-dinitro-6-phenylphenanthridine {**5p**} was done primarily by examining splitting patterns, coupling constants and the COSY spectrum, because the chemical shifts are more complicated (see figure 52 and figure 35). The main exception is that the protons of the phenyl substituent are the most

upfield, because that ring does not have any electron-withdrawing nitro groups on it, unlike the phenanthridine system; and also because the two ring systems are not co-planar, due to steric repulsion (similarly to the previous biphenyl compounds), so their π-systems are separate. For this reason, and also because of the large number of bonds between them (six at the closest), no coupling is observed between the phenyl (**30'**, **31'** & **32'**) and phenanthridinyl (**17'**, **19'**, **20'**, **23'**, **24'** & **26'**) protons.

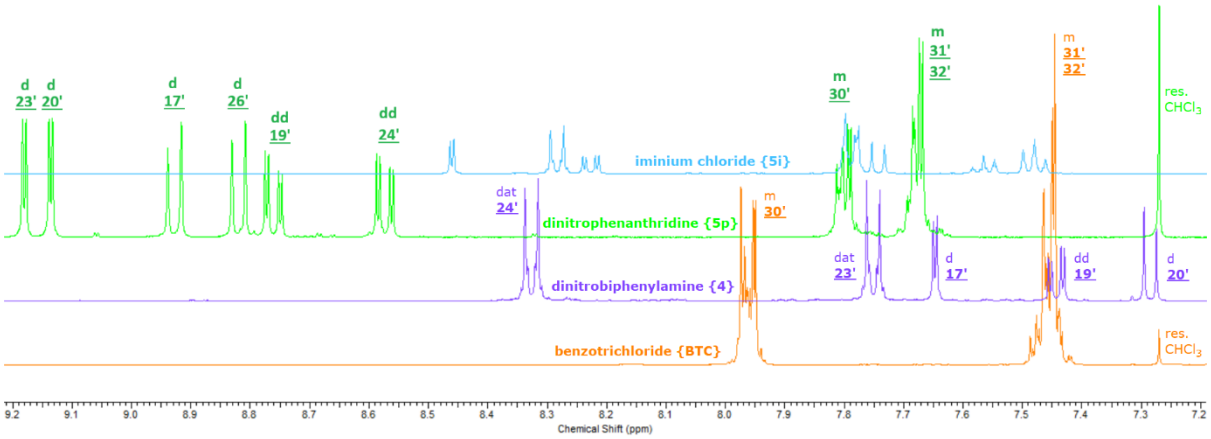

Figure 52: ^{1}H NMR comparison of starting materials and product of benzcyclization.

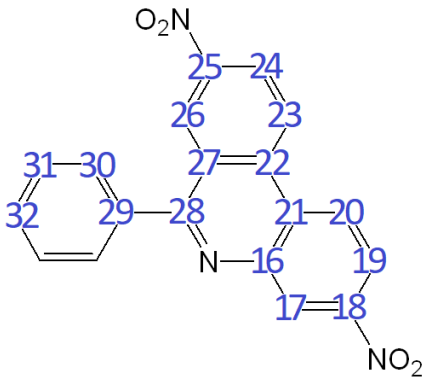

Figure 35: arbitrarily numbered structure of the phenanthridine {**5p**}.

Nonetheless, with respect to the phenyl ring, the dinitrophenanthridinyl substituent does have a moderate electron-withdrawing effect by induction. This effect is only really felt by the protons nearest to the substituent, **30'**, which must therefore correspond to the most downfield peak that has a relative integral of 2H: the complex doublet of doublets at 7.80 ppm. The first-order doublet is due to coupling with its vicinal neighbour **31'**, the second-order doublet due to long-range coupling to **32'**, and the additional complexity—which couldn't be resolved—arises from the fact that (similarly to the biphenyl compounds discussed previously) the chemical environments are not exactly the same on either side of the line of symmetry, because there is a barrier to rotation around bond **28**–**29** and the minimum-energy torsion angle between the rings is not 90°. Protons **31'** and **32'** are not significantly deshielded, so their peaks coincide further upfield, at 7.68 ppm.

The phenanthridine moiety is almost symmetrical, which results in three pairs of peaks; a pair consisting of two separate peaks, each with the same splitting pattern and coupling constants and similar (but not identical) chemical shift as the other. These correspond to protons that are opposite one another with respect to the line of (near) symmetry. Due to the large number of bonds between them (five at the closest), no coupling is observed between protons that are on different rings or that are *para* to each other. There is vicinal coupling between **19'** and **20'**, and between **23'** and **24'**; and there is long-range coupling between *meta* protons: **17'** with **19'**, and **24'** with **26'**. Two of the six peaks (or one of the three pairs) are split into doublets of doublets, which must correspond to **19'** and **24'**, as they each couple to two other protons. The remaining four peaks (two pairs) are all doublets; one pair has a visibly larger coupling constant than the other, due to stronger vicinal coupling, so these correspond to **20'** and **23'**, while the peaks with the smaller coupling constant correspond to **17'** and **26'**, which only have the weaker, long-range coupling.

Determination of which proton from each of the three pairs shared a ring with each other was done by examining the COSY spectrum: the doublet of doublets at 8.57 ppm couples with the doublets at 8.82 and 9.18 ppm, while the doublet of doublets at 8.76 ppm couples with the doublets at 8.93 and 9.14 ppm.

Similarly to the nitration reaction {**ABP→4**}, the most noticeable change in the ^{1}H NMR of the phenanthridine {**5p**} compared to 4,4'-dinitro-2-aminobiphenyl {**4**} is a strong deshielding effect: all six protons on the phenanthridine ring system are 1-2 ppm further downfield than they were in the primary amine. This can be attributed to two factors. The first is that a primary amino nitrogen has become part of a pyridine ring. Both are inductively withdrawing, but whereas the lone pair of the primary amine could mesomerically donate to the adjacent arene, that of the pyridine nitrogen cannot: it occupies an sp^2 orbital than doesn't overlap with the ring π-system, so no resonance donation is possible. Therefore, adjacent atoms in the phenanthridine experience the full effect of the nitrogen atom's inductive withdrawal. This also explains why **17'** is more downfield than **26'**: the former is closer to the pyridine nitrogen atom, and the strength of this inductive effect drops off rapidly with distance.

The second factor is the formation of a fused ring system which enhances the ring current effect. On application of an external magnetic field (such as is produced by an NMR spectrometer), the circulation of π-electrons around an aromatic ring induces a diamagnetic ring current. This results in a secondary magnetic field, which may be modelled as a dipole, centred in the middle of the ring, which opposes the applied field such that protons above and below the ring are shielded, but those in the plane of the ring are deshielded. As discussed previously, the biphenyl-based starting material is

not planar: there is an oblique angle between the plane of the two rings, so each has a separate π-system that cannot overlap with its neighbour.

However, after benzcyclization, those two rings are forced to be co-planar as they are incorporated into the new three-ring phenanthridine moiety, which is a unified aromatic system. Every proton within that system now experiences not only the magnetic field produced by its own ring, but part of the neighbouring ring's field too, so they are all more deshielded than they were in the biphenyl-based starting material. Ring current also explains why **20'** and **23'** are further downfield than **17'**, **19'**, **24'** and **26'** even though the latter are closer to the strongly electron-withdrawing nitro groups: in a system of fused aromatic rings, protons that are closer to the ring fusion carbons are more deshielded than other protons on the same ring, because they experience more of the neighbouring ring's field.

COUPLING LINKER AT NITROGEN {3+4→7}

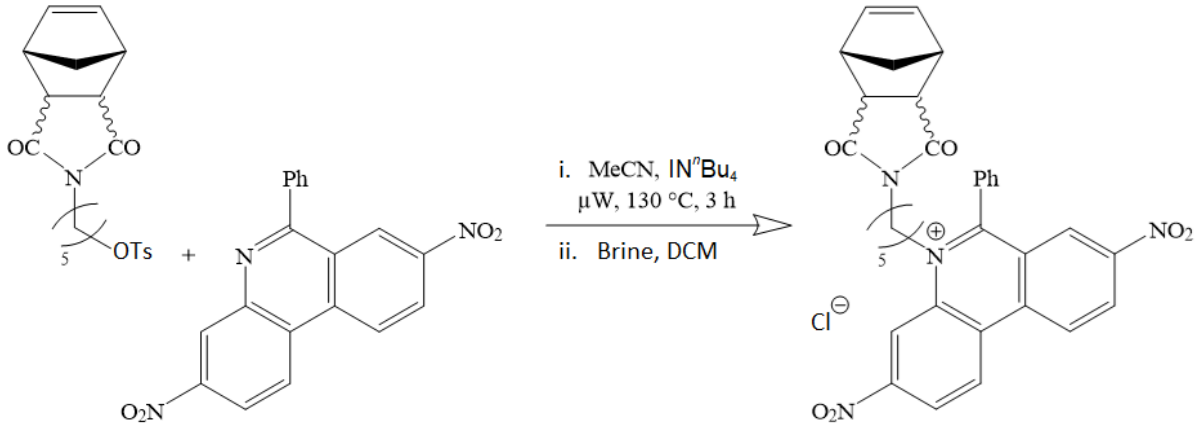

Figure 53: coupling tosylate {**3**} with phenanthridine {**5p**} to form the nitro-himide {**8**} failed.

The most challenging step in the synthesis was to couple a suitably functionalised himide-linker compound to the nucleophilic nitrogen centre of an EthBr precursor compound. The first combination to be tested was the already-synthesised tosylate and phenanthridine (see figure 53). However, heating to 160 °C, adding tetrabutylammonium iodide as a catalyst and even using a microwave reactor all failed to start the reaction. When the temperature was raised significantly higher or the reaction left for much longer than a day, the norbornene moiety was destroyed. Three possible explanations for the failure of this reaction were identified, as detailed below.

1st explanation—That the himide moiety may share intermolecular interactions with the phenanthridine of sufficient strength to cause the two to be permanently in

close proximity, sterically hindering the nucleophile from meeting the electrophilic carbon. This possibility was excluded as the principal problem by producing ethyl tosylate and then trying—and failing—to couple it (instead of the himide-tosylate) to the phenanthridine, using the same method as before.

2nd explanation—That the tosylate moiety may not be a good enough leaving group (though it is one of the best) or that it is sterically shielding the electrophilic carbon from the nucleophile. Either way, this would require the use of a smaller and better leaving group; ethyl mesylate was prepared and it failed to couple with the phenanthridine. *Ethyl* mesylate was used (instead of the mesylate of the himide) in order to eliminate the possibility that explanations #1 and #2 were both contributing significantly to the failure of the reaction.

3rd explanation—Having ruled-out the first two possible problems (which would have been the easiest to fix), it was then decided to focus on finding a solution to the most likely explanation of the problem: that the supposedly nucleophilic nitrogen atom is actually not very nucleophilic. This is because it exists in an aromatic system that is bonded to two nitro-groups, which strongly withdraw electron-density from the rings, and by extension, from that phenanthridine nitrogen atom. Three possible solutions to this problem were attempted, starting with the easiest to implement.

1st solution—The benzcyclization intermediate that was isolated previously had not degraded in the intervening months—unusually for an imidoyl chloride—which may be because it was kept as the hydrochloride salt, which ought to make that functional group less vulnerable to hydrolysis in the moist air. The free base of this compound was acquired in the hope that it would be a better nucleophile, due to it no longer sharing an aromatic system with two nitro-groups, but only one.

However, the reaction only produced the original hydrochloride salt. This may be because triethylammonium chloride from making the free base was not removed prior to the attempted coupling reaction, allowing it to react with ethyl tosylate to form tosic acid, which would re-protonate the free base. The appeal of the 1st solution was then negated by the fact that there was insufficient material left with which to re-attempt it.

Regardless, this was never a particularly promising approach, because the primary cause of the nucleophilic nitrogen's poor nucleophilicity is that in both this molecule and in the phenanthridine, it is sp^2 hybridised and shares a π-bond with an aromatic ring, *meta* to a nitro group. This resonance strongly withdraws from the nucleophile.

2nd Solution—The nitro- groups would be reduced to amines first, then protected with a suitable protecting group (to be determined), before the coupling reaction is performed, and then the amines de-protected. As long as the reduction could be

completed without issue, the rest should be feasible (if time-consuming), because the nucleophile should then be actually nucleophilic, with both electron-withdrawing nitro- groups replaced with electron-donating amines. However, the reduction did not work, as discussed in the following section, and the 2nd solution was abandoned for lack of time.

3rd solution—The solution that ultimately worked was to first couple the tosylate {**3**} to 4,4'-dinitro-2-aminobiphenyl {**4**}, then perform the benzcyclization on the resulting secondary amine compound {**7**} to yield the dinitro-himidium compound {**8**}, i.e. switching the order in which those two reactions are done (see Figure 54). There was a concern that the linker would induce the secondary amine product to be an even better nucleophile than the starting material, but presumably steric hindrance prevented that, because there was no significant di-substitution.

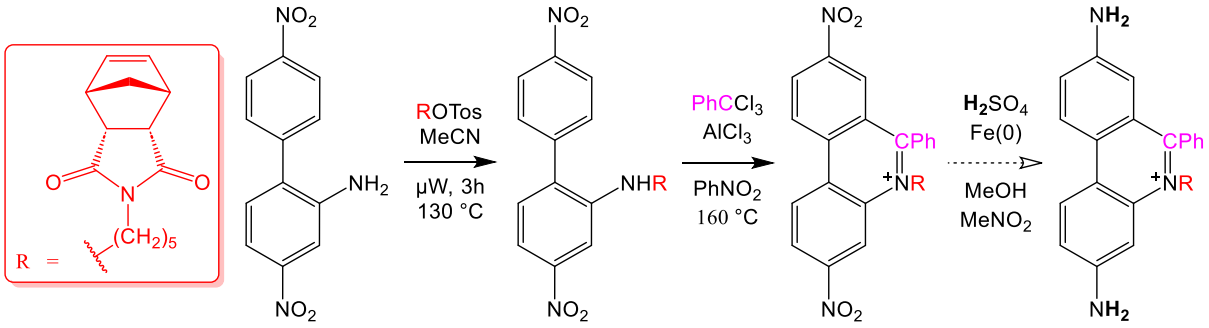

Figure 54: the 3rd solution {**3+4→7→8**}; note the final reduction {**8→HimCl**} was not attempted.

Due to time constraints, the secondary amine {**7**} product of the coupling reaction was not analysed, but instead the benzcyclization was performed on it, yielding the dinitro-himidium compound {**8**}, as identified by LC-MS (see experimental). The final reaction prior to polymerization was to be a Béchamp reduction to yield the monomer, N-(5-(3,8-diamino-6-phenylphenanthridinyl)-pentyl)-himidium chloride {**HimCl**}, but it was not attempted due to lack of time.

CONCLUSIONS

ACHIEVEMENTS

The motivating purpose of undertaking this work was to learn how to conduct independent chemical research, which was achieved: in addition to the laboratory experience acquired, the numerous failed reactions taught a lesson in humility, perseverance and lateral thinking.

While the principal aim of the project—to develop and test a novel kind of nucleic acid vector to afford targeted cell transport—was not achieved due to lack of time, good progress was made towards that aim, and no indication was found that it could not be achieved, given more time.

Thermal isomerisation of *endo*-himic anhydride into its *exo* diastereomer and subsequent purification to 98% by threefold recrystallisation was reproduced with a good yield of 11%, and an amino-alcohol linker was attached to each of these diastereomers. The procedures previously used by members of the Biagini group were employed in these reactions, without complication. Nitration of 2-aminobiphenyl in the 4 and 4' (systematic numbering) positions was conducted without issue as described in the literature.

Tosylation of the himidols using DMAP catalyst yielded two previously unreported compounds. The subsequent benzcyclization was successful using aluminium chloride as the catalyst and nitrobenzene as solvent, which is a slightly different procedure from what has been done previously. Under milder conditions, an iminium chloride salt was isolated as an intermediate, which suggests that the benzcyclization proceeds by N-substitution first, followed by the Friedel-Crafts, which contradicts the pathway suggested in 1950 by Barber et al.[19]

The first three objectives of the project were achieved, to find a viable pathway for the total synthesis of the himidium chloride monomer. The monomer itself was not produced, but an immediate precursor to it was, requiring only a single further reaction to reduce the aromatic nitro groups to anilines and yield the monomer.

FUTURE RESEARCH

Below is outlined some further work that may be done to continue investigating norbornene-based poly(intercalator) systems as possible DNA vectors.

The norbornene—EthBr adduct could be reduced by a Béchamp reduction using iron powder and sulfuric acid to reduce the aromatic nitro groups to anilines. The preferred modern method of catalytic hydrogenation would be infeasible in this case due to the presence of an alkene group that must be preserved.

Ring-opening metathesis polymerisation (ROMP) would be performed on the resulting monomer, to form a block co-polymer with a different norbornene adduct, the chemistry of which would control the vector's specificity.

Prior research has demonstrated that norbornene—poly(ethylene glycol) ROMP polymers can self-assemble into micelle-like nanoparticles, so that would be a sensible first adduct to try to co-polymerise with the EthBr one. Following the procedure from aforementioned research: the EthBr monomer is stirred at room temperature for ten minutes in dry DCM with a third-generation Grubbs catalyst, then an equimolar quantity of a PEG-norbornene monomer is added, and the co-polymerisation is terminated ten minutes later with ethyl vinyl ether.[20]

Investigation of the vector's fluorescence when binding DNA and selectivity in transporting it across cell membranes would follow. Depending on the results, alternative nucleic acid intercalators could be explored.

REFERENCES

[1] Karol Langner, *Ethidium intercalated between two adenine-thymine base pairs*, **2024**, *Dec. 28*, https://en.wikipedia.org/wiki/Intercalation_(biochemistry).

[2] P Bertrand, C Blanquart and V Héroguez, *Biomolecules*, **2019**, *9*(2), Art. 60.

[3] S Shehata, C J Serpell and S C G Biagini, *Mater. Today Commun.*, **2020**, *25*, Art. 101562.

[4] K Xiu, J Zhang, J Xu, Y E Chen and P X Ma, *Biophysics Rev.*, **2023**, *4*(1), Art. 011313.

[5] S Bhaduri, N Ranjan and D P Arya, *Beilstein J. Org. Chem.*, **2018**, *14*, 1051–1086.

[6] R Galindo-Murillo and T E Cheatham III, *Nucleic Acids Res.*, **2021**, *49*(7), 3735–3747.

[7] Piet Borst, *IUBMB Life*, **2005**, *57*(11), 745–747.

[8] P Payamyar, B T King, H C Öttinger and A D Schlüter, *Chem. Commun.*, **2016**, *52*, 18–34.

[9] N M L Hansen, K Jankova and S Hvilsted, *Eur. Polym. J.*, **2007**, *43*, 255–293.

[10] WikiChemist2013, *The catalytic cycle of a living ring-opening metathesis polymerization*, **2024**, *December 28th*, https://en.wikipedia.org/wiki/Living_polymerization#Living_ring-opening_metathesis_polymerization.

[11] S C G Biagini, M P Coles, V C Gibson, M R Giles, E L Marshall and M North, *Polymer*, **1998**, *39*, 1007–1014.

[12] Ioannis Choinopoulos, *Polymers*, **2019**, *11*(2), Art. 298.

[13] L T Birchall, S Shehata, C J Serpell, E R Clark and S C G Biagini, *J. Chem. Educ.*, **2021**, *98*, 4013–4016.

[14] L T Birchall, S Shehata, S McCarthy, H J Shepherd, E R Clark, C J Serpell and S C G Biagini, *Polym. Chem.*, **2020**, *11*, 5279–5285.

[15] Lee T Birchall, Synthesis of monomers for Ring-Opening Metathesis Polymerisation (ROMP): Optimisation and attachment of fluorophores, **2019**, University of Kent, Canterbury (MSc).

[16] M. Hara, Y. Odaira And S. Tsutsumi, *Tetrahedron*, **1966**, *22*, 95–100.

[17] K K W To, X Wang, C W Yu, Y-P Ho and S C F Au-Yeung, *Bioorg. Med. Chem.*, **2004**, *12*(17), 4565–4573.

[18] J Cymerman and W F Short, *J. Chem. Soc.*, **1949**, 703–707, Art. 150.

[19] H J Barber, L Bretherick, E M Eldridge, S J Holt and W R Wragg, *J. S. C. I.*, **1950**, *69*, 82–96.

[20] Sara Shehata, Synthesis of ROMP polymers for biological applications, **2023**, University of Kent, Canterbury (PhD).

BIBLIOGRAPHY

[21] N Appukutti, J R Jones and C J Serpell, *Chem. Commun.*, **2020**, *56*, 5307–5310.

[22] X Cai, L Ji, H Tang, R Wang and F Feng, *Chem. Commun.*, **2021**, *57*(92), 12313–12316.

[23] J F Chiang, R Chiang, K C Lu, E-M Sung and M D Harmony, *J. Mol. Struct.*, **1977**, *41*, 67–77.

[24] N H Evans, C J Serpell and P D Beer, *Angew. Chem. Int. Ed.*, **2011**, *50*, 2507–2510.

[25] X Huang, G Wu, C Liu, X Hua, Z Tang, Y Xiao, W Chen, J Zhou, N Kong, P Huang, J Shi and W Tao, *Nano Lett.*, **2021**, *21*(22), 9706–9714.

[26] G W Kabalka, M Varma and R S Varma, *J. Org. Chem.*, **1986**, *51*, 2386–2388.

[27] T Konakahara, R L Wurdeman and B Gold, *Biochemistry*, **1988**, *27*, 8606–8613.

[28] U J Krull, P A Piunno, R H E Hudson, M Damha and A H Uddin, *Nucleic Acid Biosensor Diagnostics*, **1998**, *Patent Application Num. PCT/CA1998/000402*, Publication Num. WO/1998/058079.

[29] P Laszlo and P v R Schleyer, *J. Am. Chem. Soc.*, **1964**, *86*(6), 1171–1179.

[30] C Lion, J P Boukou-Poba and C Charvy, *Bull. Soc. Chim. Belg.*, **1990**, *99*(3), 171–181.

[31] C Navarro-Ranninger, E I Montero, I López-Solera, J R Masaguer and B Lippert, *J. Organomet. Chem.*, **1998**, *558*, 103–110.

[32] S A Osadchii, V G Shubin, L P Kozlova, V S Varlamenko, M L Filipenko and U A Boyarskikh, *Russ. J. Appl. Chem.*, **2011**, *84*(9), 1541–1548.

[33] B Pandey, A A Athawale, R S Reddy, P V Dalvi and P Kumar, *Chem. Lett.*, **1991**, *20*(7), 1173–1176.

[34] Ernest Ritchie, *JProcRSNSW*, **1944**, *78*(3), 164–168, Art. 20.

[35] C J Serpell, R N Rutte, K Geraki, E Pach, M Martincic, M Kierkowicz, S De Munari, K Wals, R Raj, B Ballesteros, G Tobias, D C Anthony and B G Davis, *Nat. Commun.*, **2016**, *7*, Art. 13118.

[36] C J Serpell, A Y Park, C V Robinson and P D Beer, *Chem. Commun.*, **2021**, *57*, 101–104.

[37] K Todoroki, Y Hamashima, H Egami, S Nakagawa, T Sakai, O Inoue, S Nishiyama, M Kanazawa and H Tsukada, [*phenanthridine-based*] *compound or salt thereof*, **2021**, *Patent Application Num. PCT/JP2020/041254*, Publication Num. WO/2021/090850.

[38] Leslie P. Walls, *J. Chem. Soc.*, **1945**, 294–300, Art. 78.

[39] T R Wilks, A Pitto-Barry, N Kirby, E Stulz and R K O'Reilly, *Chem. Commun.*, **2014**, *50*(11), 1338–1340.